PLOS PATHOGENS

RESEARCH ARTICLE

Autoimmunity-associated allele of tyrosine phosphatase gene *PTPN22* enhances anti-viral immunity

Robin C. Orozco[1,2]*, Kristi Marquardt[1], Isaraphorn Pratumchai[1], Anam Fatima Shaikh[2], Kerri Mowen[1†], Alain Domissy[3], John R. Teijaro[1], Linda A. Sherman[1]*

1 Department of Immunology and Microbiology, Scripps Research, La Jolla, California, United States of America, **2** Department of Molecular Biosciences, University of Kansas, Lawrence, Kansas, United States of America, **3** Genomics Core, Scripps Research, La Jolla, California, United States of America

† Deceased.
* Orozco.robin@ku.edu (RCO); lsherman@scripps.edu (LAS)

Citation: Orozco RC, Marquardt K, Pratumchai I, Shaikh AF, Mowen K, Domissy A, et al. (2024) Autoimmunity-associated allele of tyrosine phosphatase gene *PTPN22* enhances anti-viral immunity. PLoS Pathog 20(3): e1012095. https://doi.org/10.1371/journal.ppat.1012095

Editor: Zia Rahman, Thomas Jefferson University, UNITED STATES

Received: April 26, 2023

Accepted: March 4, 2024

Published: March 21, 2024

Data Availability Statement: Data used in this manuscript is uploaded to Dryad Repository (DOI: 10.5061/dryad.msbcc2g55). RNA sequencing data is available at GEO Accession number: GSE255614) https://www.ncbi.nlm.nih.gov/geo/query/acc.cgi?acc=GSE255614).

Funding: Research reported in this publication was supported by the National Institute of General Medical Sciences (NIGMS) of the National Institutes of Health under award number P20GM113117 (awarded to R.C.O, while at

Abstract

The 1858C>T allele of the tyrosine phosphatase *PTPN22* is present in 5–10% of the North American population and is strongly associated with numerous autoimmune diseases. Although research has been done to define how this allele potentiates autoimmunity, the influence *PTPN22* and its pro-autoimmune allele has in anti-viral immunity remains poorly defined. Here, we use single cell RNA-sequencing and functional studies to interrogate the impact of this pro-autoimmune allele on anti-viral immunity during Lymphocytic Choriomeningitis Virus clone 13 (LCMV-cl13) infection. Mice homozygous for this allele (PEP-619WW) clear the LCMV-cl13 virus whereas wildtype (PEP-WT) mice cannot. This is associated with enhanced anti-viral CD4 T cell responses and a more immunostimulatory CD8α$^-$ cDC phenotype. Adoptive transfer studies demonstrated that PEP-619WW enhanced anti-viral CD4 T cell function through virus-specific CD4 T cell intrinsic and extrinsic mechanisms. Taken together, our data show that the pro-autoimmune allele of *Ptpn22* drives a beneficial anti-viral immune response thereby preventing what is normally a chronic virus infection.

Author summary

PTPN22 and its alternative allele, 1858C>T, has largely been studied in the context of autoimmunity. Through these studies, researchers defined roles for *PTPN22* in regulating T lymphocyte activation, myeloid cell cytokine production, and macrophage polarization. Despite these immune pathways being critical for anti-viral immunity, little work has studied how this allele impacts virus infection. In this study, we examine gene expression and function of immune cell subsets to demonstrate how a common allelic variant of *PTPN22*, which strongly increases the risk of autoimmune disease, promotes successful clearance of an otherwise chronic viral infection.

University of Kansas) and NIH U01 AI130842 (awarded to L.A.S) and NIH T32 AI007354 27 (fellowship to support R.C.O, while at Scripps). The funders had no role in study design, data collection and analysis, decision to publish, or preparation of the manuscript.

Competing interests: The authors have declared that no competing interests exist.

Introduction

Allelic variation in genes that regulate immune cell responses potentially impact an individual's response to self and foreign antigens. Genome wide association studies (GWAS) have identified variants in immune-related genes that are being increasingly associated with protective or pathologic consequences during disease [1]. However, the underlying mechanism(s) through which these mutations impact disease often remain incompletely defined.

The 1858C>T allele of the tyrosine phosphatase *PTPN22 (*causing amino acid substitution R620W) is present in 5–10% of the North American population and is strongly associated with numerous autoimmune diseases, including Type I Diabetes (T1D), rheumatoid arthritis, systemic lupus erythematosus, and others [2–10]. This alternative allele of *PTPN22* is considered the highest non-HLA risk allele in autoimmunity [7,9]. This pro-autoimmune allele is known to affect innate and adaptive immune functions, including, lymphocyte activation, toll-like receptor signaling, and cytokine production in various autoimmune contexts [8,11–18]. In humans, *PTPN22* encodes the protein Lyp that is expressed in all immune cells [10]. To study its function in immune cell types, researchers have often employed *Ptpn22* knock-out mice, which are deficient in expression of the Lyp ortholog, PEP (PEP-null) [20]. In lymphocytes, Lyp/PEP tempers T cell receptor (TCR) and B cell receptor (BCR) signaling through dephosphorylation of Src kinases. Binding partners enabling such activity include TRAF3 and CSK [12,14]. In myeloid cells, the interaction of Lyp/PEP with TRAF3 promotes TLR activation and type I interferon production [11,15]. Through these studies, researchers have identified mechanisms that may contribute to the pathogenesis of multiple autoimmune disorders. Despite the importance of these same immune regulatory factors in shaping a robust anti-viral immune response, the impact of the pro-autoimmune allelic variant of *PTPN22* on anti-viral immunity has received far less attention.

One of the best-defined experimental models of persistent virus infection is the lymphocytic choriomeningitis virus clone 13 (LCMV-cl13) model in C57BL/6 mice [21–23]. Using LCMV clone 13 (LCMV-cl13) researchers have defined mechanisms of viral persistence and immune cell exhaustion [23–26]. Previously we and others found that, upon infection with LCMV-cl13, mice lacking *Ptpn22* (PEP-null) have accelerated viral clearance and exhibit less of an exhausted T cell phenotype [27,29]. Specifically, there was enhanced anti-viral CD4 T cell function and improved CD8 T cell function late in infection, suggesting *Ptpn22* contributes to the generation of T cell exhaustion. However, these studies were performed using PEP-null mice rather than mice expressing the equivalent of the human pro-autoimmune allele. Therefore, it remained to be determined whether the alternative human allele would similarly contribute to viral clearance and immune effector functions.

In this study, we use C57BL/6 mice mutated using CRISPR/Cas9 to express the murine ortholog of the *Ptpn22* pro-autoimmune allele (PEP-619WW) and LCMV-cl13 to define new mechanisms by which the autoimmunity associated allele of *PTPN22* contributes to viral clearance and enhances anti-viral T cell and myeloid cell responses.

Results

Ptpn22 alternative allele promotes LCMV-cl13 viral clearance

Mice expressing the *Ptpn22* wild type allele (PEP-WT) or *Ptpn22* pro autoimmune allele (PEP-619WW) were infected with LCMV-cl13. All mice lost weight within the first week of infection (Fig 1A). However, PEP-619WW mice stabilized and regained their original weight more quickly than PEP-WT mice (Fig 1A). This difference also correlated with viral titers in the serum of these animals (Fig 1B). While PEP-WT mice had detectable virus in their serum out

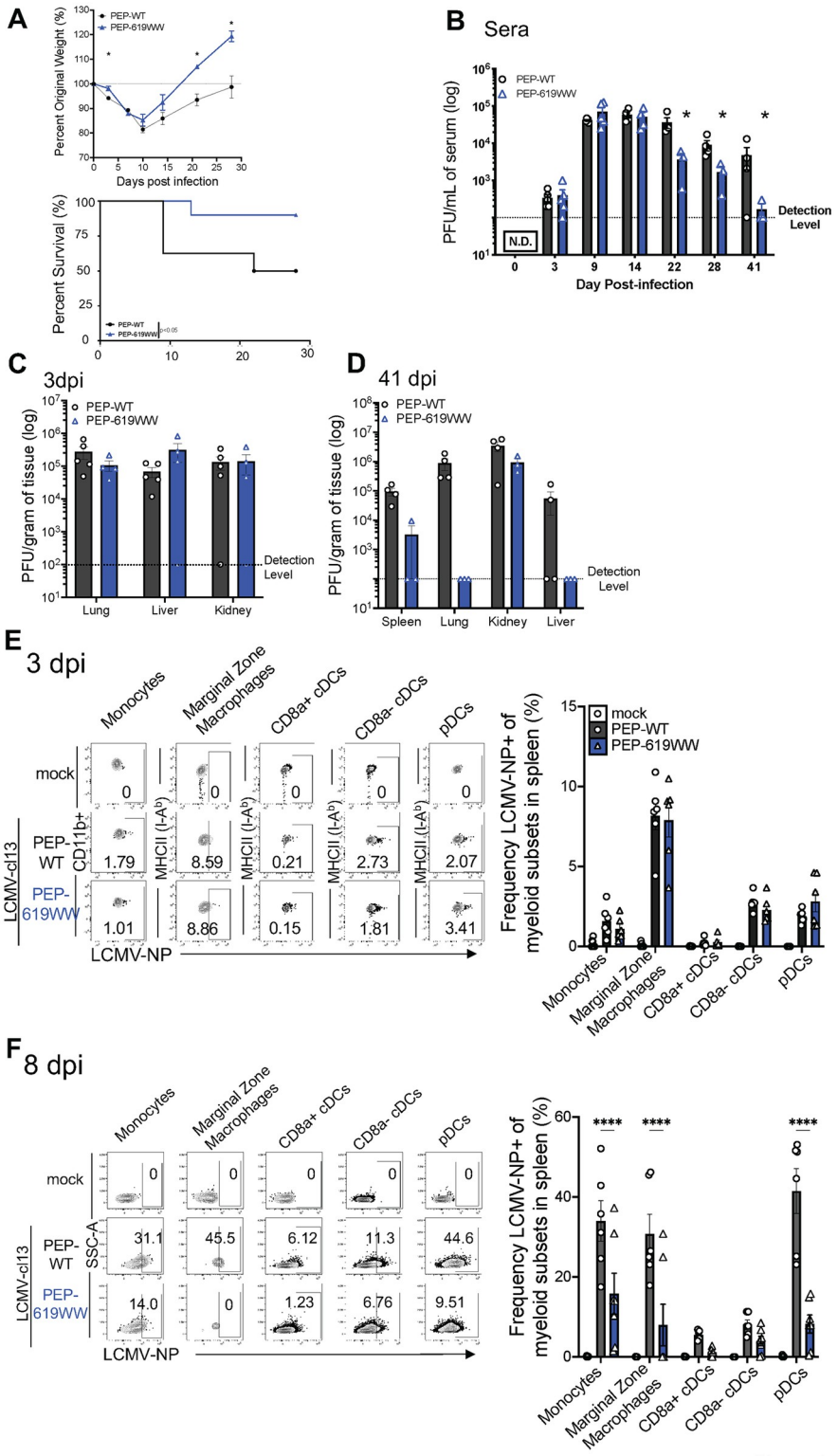

Fig 1. PEP-619WW mice have improved LCMV-cl13 control over PEP-WT mice. C57BL/6 mice with wild type (PEP-WT, black) or pro autoimmune allele (PEP-619WW, blue) *Ptpn22* gene were infected with 1x10^6 PFU chronic viral strain LCMV-clone 13 (LCMV-cl13) (i.v). On indicated days mice were weighed (A), and bled for serum titer (B). Viral load was determined at early (3dpi, C) and late (41dpi, D) within target organs. Using flow cytometry presence of LCMV nucleoprotein (LCMV-NP) (clone VL-4) was determined in multiple myeloid cell subsets at day 3 (E) and day

8 (F). Representative flow plots (which is the median mouse data point in corresponding bar graph) shows LCMV-NP + cells for different splenic myeloid subset at each time timepoint for mock infected (white bar, circle), infected PEP-WT (black bar, circle), and infected PEP-619WW mice (blue bar, triangles) Quantification for Frequency of LCMV-NP+ cells in corresponding bar graph to the right. Gating strategy for all *myeloid subsets* is: Lymphocytes> Single cell x2> autofluorescent- >Live> CD3- CD19-> Ly6G- CD11b+/-> (non-neutrophils) > NK1.1- (non NK). *Monocytes*: myeloid cells> F4/80+ CD11c-> Ly6C+ CD11b+. *Marginal Zone Macrophage*: myeloid cells> F4/80 + CD11c-> Ly6C- CD11b+> CD209b+. *CD8α+ cDCs*: myeloid cells> F4/80- >CD11c+ PDCA-1- CD8α+. *CD8α- cDCs*: myeloid cells> F4/80- >CD11c+ PDCA-1- CD8α-. *pDCs*: myeloid cells> F4/80- > CD11c+/- PDCA-1+. Weight loss studies pooled from 3 separate experiments: Starting group sizes were PEP-WT n = 15, PEP-619WW n = 19. Serum titer, tissue titer from representative experiment. Each dot indicates an individual mouse. Each dot represents an individual mouse and is from pooled experiments. SEM shown. $^{*}p<0.05$, $^{**}p<0.01$, $^{***}p<0.001$, $^{****}p<0.0001$, Two Way ANOVA with Sidak Post Hoc Analysis.

https://doi.org/10.1371/journal.ppat.1012095.g001

to day 41, viral titer in PEP-619WW mice decreased by 22 days post infection (dpi) (Fig 1B). PEP-619WW did not restrict early LCMV-cl13 infection, as viral loads in both genotypes of mice were high 3 dpi in sera, lungs, livers, and kidneys (Fig 1B and 1C). By day 41, PEP-619WW mice had no detectable virus in the serum and largely cleared virus from the target organs spleen, lungs, and livers (Fig 1D). In contrast, PEP-WT mice still had detectable virus in these organs. In both strains of mice, virus was still detectable in the kidney, an organ in which it is known virus remains detectable despite clearance from other organs [22,23,30,31].

Cellular tropism is thought to be a key factor in determining the potential chronicity of a virus infection [25,31]. Specifically, the ability to establish a persistent infection in C57BL/6 mice is attributed to the increased capacity of LCMV- cl13 to infect dendritic cells (DCs) and macrophages, including plasmacytoid DCs (pDCs) and marginal zone macrophages [25,31–34]. To determine if PEP-619WW mice had altered tropism we examined LCMV nucleoprotein (NP) expression in multiple myeloid cell subsets. At 3 dpi, no difference was detected in LCMV-NP+ cells amongst monocytes (Ly6C+ CD11b+, Ly6G-), marginal zone macrophages (Ly6C- CD11b+ CD209b+, F4/80+), $CD8\alpha^{+}$ conventional dendritic cells (cDCs) (CD11c+, PDCA-1-, MHC II (I-Ab)+, CD8a+), $CD8\alpha^{-}$ cDCs (CD11c+, PDCA-1-, MHC II (I-Ab)+, CD8a-), or pDCs (CD11c+/-, PDCA-1+, Ly6C+, B220+) (Fig 1E). By 8 dpi, PEP-619WW mice had a significantly decreased proportion of LCMV-NP+ splenic monocytes, marginal zone macrophages, and pDCs (Fig 1F). There was also a lower proportion of $CD8\alpha^{+}$ cDCs that were LCMV-NP+ cells, but this did not reach significance. We did not observe any difference in the proportion of LCMV-NP+ $CD8\alpha^{-}$ cDCs (Fig 1F). At 8 dpi, the marginal zone macrophages from most PEP-619WW mice had no detectable virus (Fig 1F). However, in 2 PEP-619WW animals, about 20–30% of marginal zone macrophages were LCMV-NP+ (Fig 1F). This is in sharp contrast to PEP-WT mice, where 20–50% of marginal zone macrophages were LCMV-NP+ (Fig 1F). Thus, despite no detectable difference in viral tropism early after infection between PEP-WT and PEP-619WW mice, there is accelerated clearance of virus from PEP-619WW mice, which was evident as early as 8 dpi in some cell types.

Immune cell heterogeneity in PEP-619WW mice during virus infection

To better understand how the *Ptpn22* alternative allele is impacting anti-viral immunity, we globally characterized all immune cells in the spleen 8dpi (Fig 2A). Live immune cells (CD45 +) sorted from 8 dpi infected PEP-WT and PEP-619WW mice were used for single cell RNA sequencing (scRNAseq) using 10x Genomics platform (Fig 2A). Expression of *Cd45* confirmed most cells sequenced were immune cells (Fig 2B). Using *Csfr1*, *Ly6G*, *Cd19*, and *Cd3e* expression we were able to visualize clustering of monocytes, neutrophils, B cells, and T cells, respectively (Fig 2C). Next, based on these markers we reclustered the specific cell populations to group transcriptionally similar cells and then we compared the proportion of each new cluster

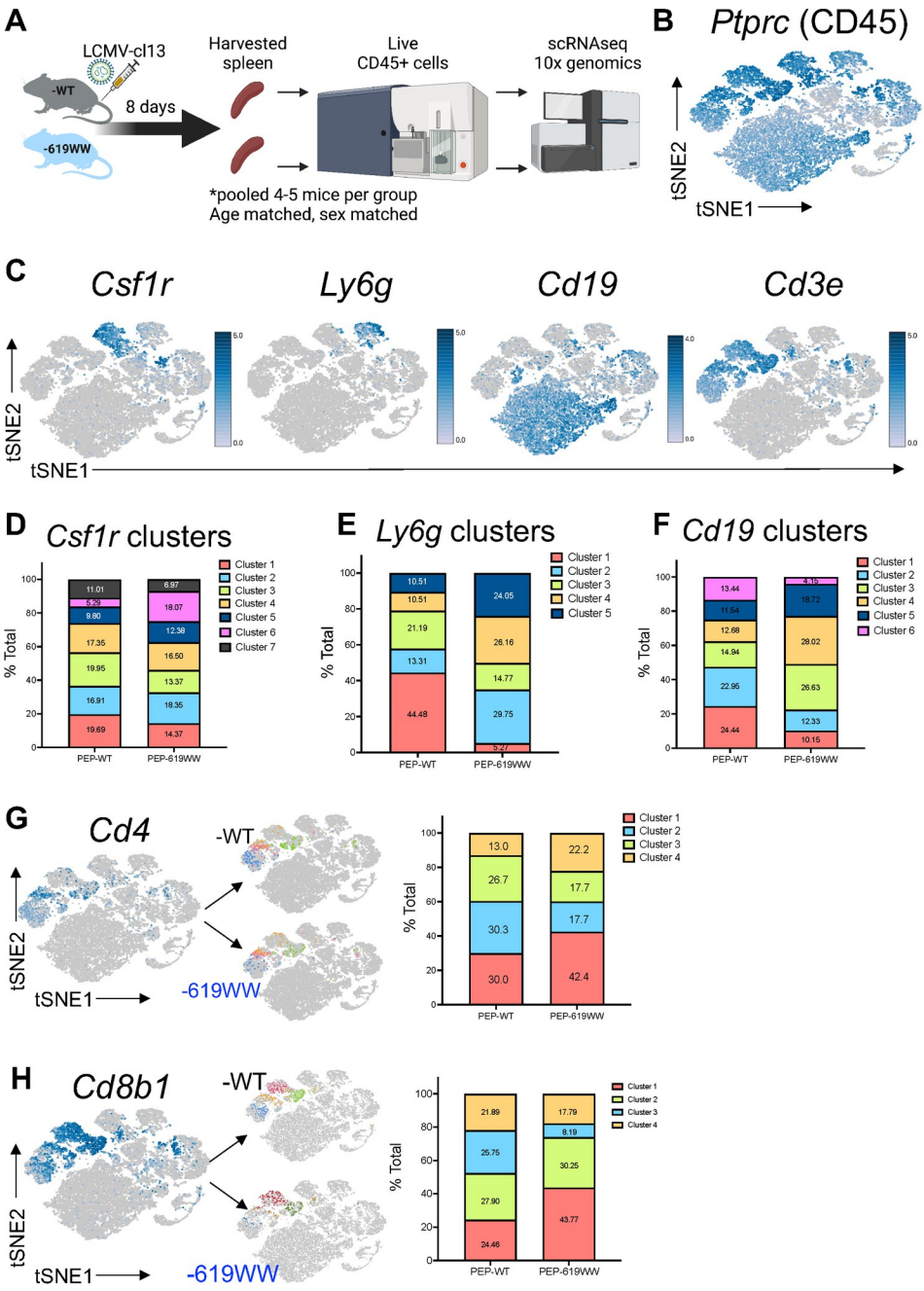

Fig 2. PEP-619WW mice have transcriptionally distinct immune cell subsets from PEP-WT mice during LCMV-cl13 infection. At 8dpi, pooled splenocytes (by genotype) from age matched, sex matched mice were sorted for live CD45+ cells and submitted for single cell RNA sequencing (scRNAseq) on the 10x genomic platform (diagram created with biorender.com)(A). Relative gene expression of *Ptprc* indicating immune cell in aggregated data set (both genotypes) (B). Relative gene expression to located immune cell clusters of myeloid *Csfr1*, neutrophil *Ly6g*, B cell *Cd19*, and T cell *Cd3e* (C). Using Loupe software, each population was reclustered to group like cell subsets among the larger cell type and the proportions compared between genotypes. The frequency of each cluster among total cell population is listed on the graph. Myeloid cell cluster, based on *Csf1r* expression (D), Neutrophil clusters, based on *Ly6g* expression (E), and B cell cluster, based on *Cd19* expression (F). T cells were further broken down into CD4 T cells (expression of *Cd3e*>0, *Mt2*<10, *Cd4*>0) (G) and CD8 T cells (expression of *Cd3e*>0, *Mt2*<10, *Cd8b1*>0) (H). tSNE plots highlighting *Cd4* (G) and *Cd8b1* (H) as well as breakdown of cluster for each T cell type in -WT and -619WW cells. Corresponding quantification of proportion of either CD4 T cells or CD8 T cell subsets is next to tSNE plot.

https://doi.org/10.1371/journal.ppat.1012095.g002

within each genotype. Amongst *Csfr1* expressing monocytes 7 unique clusters were identified. Cluster 6 demonstrated the greatest difference in proportion between PEP-WT and PEP-619WW cells (Fig 2D). *Ly6G* expressing cells were grouped into 5 unique clusters, all of which were represented at different proportions in PEP-WT and PEP-619WW mice (Fig 2E). *Cd19* expressing cells were grouped into 6 unique clusters, the proportions of which also differed between PEP-WT and PEP-619WW mice (Fig 2F). These data show that PEP-WT and PEP-619WW mice have different proportions of monocytes, neutrophils, and B cell subsets present in the spleen at 8 dpi and suggests that the PEP-619WW allele pleiotropically impacts the anti-viral immune response.

CD4 T cell transcriptional identity in infected PEP-WT and PEP-619WW mice

It is well established that the clearance of LCMV is dependent on virus specific CD4 and CD8 T cell responses [35,35]. Therefore, we set out to define how the *Ptpn22* pro-autoimmune allele affected T cell populations during LCMV-cl13 infection. We identified CD4 T cell and CD8 T cells using *Cd3e* expression, in addition to *Cd4* or *Cd8b1* (Fig 2G and 2H). These populations were then clustered in an unbiased form using Loupe software and we looked at the proportion of each cluster amongst all CD4 or CD8 T cell clusters from PEP-WT or PEP-619WW mice (Fig 2G and 2H).

CD4 T cells reclustered into 4 distinct populations, which differed in proportion between PEP-WT and PEP-619WW mice (Fig 2G). Among CD4 T cells in PEP-619WW mice, cluster 1 was most represented, and made up 42.4% of CD4 T cells, whereas it represented only 30% of PEP-WT CD4 T cells (Fig 2G). Furthermore, we observed decreased proportions of cluster 2 and 3 among PEP-619WW CD4 T cells compared to PEP-WT CD4 T cells. Cluster 4 had a higher proportion of cells (22.2%) amongst PEP-619WW compared to PEP-WT (13.0%) (Fig 2G).

To learn about the phenotype and function of these CD4 T cell subsets, we looked at the top defining genes for each cluster (Fig 3A). Cluster 1 is defined by a set of T follicular helper cell (T_{FH}) genes: *Sostdc1*, *Tbc1d4*, *Izumo1r*, and *2310001h17rik* [36–42]; and activated and effector CD4 T cell genes: *Tnfsf8*, *Rgs10*, *Ypel3*, *Cd200*, and *Malt1* (Fig 3A) [43–49]. Further, we determined the expression of key TFH cell markers, the transcription factor *Bcl6* and other markers *Cxcr5* and *Pdcd1* (Fig 3B). These markers were expressed the highest in the CD4 T cell cluster 1 (Fig 3B). Increased expression of both *Cd200* and *Malt1* is associated with increased TCR signaling [47,49]. This transcriptional data suggests that cluster 1, which is higher in proportion in PEP-619WW mice, is likely comprised of T_{FH} and activated/effector-type CD4 T cells. To corroborate this, CD4 T cell cluster 1 also had relatively higher expression of the activation marker C*d44* (Fig 3B).

CD4 T cell cluster 2 exhibited high expression of naïve CD4 T cell markers *Arl4c*, *Sell*, *Gpb4*, *Il7r*, and *Rapgef6* [46,50–53](Human Protein Atlas) [46] as well as high expression of genes that are key for T cell development and lineage commitment, including *Satb1*, *Txk*, and *Lef1* [54–58] (Fig 3A). Many genes associated with cluster 3 are linked to proliferation and survival, including *Birc5*, *Hist1h1b*, *Cks1b*, *Mki67*, *Hgmn2*, *Lmnb1*, *Hgmn1*, and *Dut* [59–63] (Fig 3A). Genes upregulated in CD4 T cell cluster 4 are associated with activation (*Hopx*, *Ctla2a*, *Cxcr6*, *MS4ab4*), effector functions (*Ccl5*, *IL18r1*, *Ifngr1*), and migration/homing (*Selplg*, *Itga4*) (Fig 3A) [63–73]). Also, CD4 T cell cluster 4 is defined by expression of *Nkg7*, which is associated with cytotoxic CD4 T cell function (Fig 3A) [51]. CD4 T cell cluster 4 also had expression of *Cd44* (Fig 3B). PEP-619WW also had a higher proportion of cluster 4 cells, which transcriptionally align as cytotoxic or effector CD4 T cells. Taken together, these data suggest that in

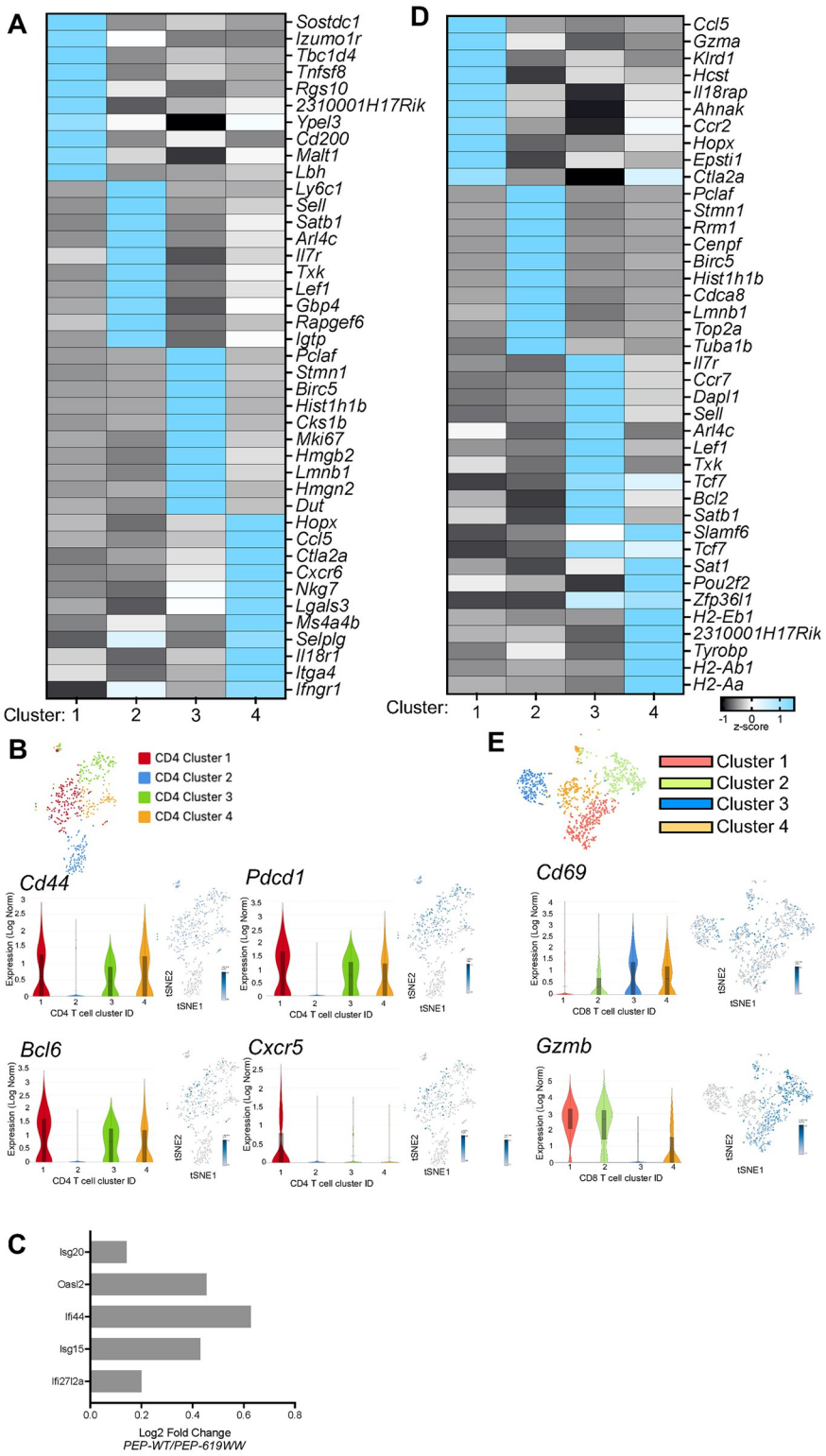

Fig 3. Top unique genes defining CD4 and CD8 T cell clusters from other clusters. Using Loupe, we identified the distinguishing gene between the CD4 T cell cluster (A) or CD8 T cell cluster (D). We then calculated the z-score of these genes across the different cluster populations within each T cell subset (-1 black, to +1 brighter blue). Genes associated with each cluster are listed. Cluster ID on bottom. Average gene expression (Log Norm) between CD4 T cell clusters of select genes *Cd44*, *Pdcd1*, *Bcl6*, and *Cxcr5* quantified and highlighted on tSNE visualization (B). Log fold

change of selected interferon inducible genes, *Isg20*, *Oasl2*, *Ifi44*, *Isg15*, and *Ifi27l2a* (C). Average gene expression of selected genes to further identify CD8 T cell clusters *Cd69* and *Gzmb* quantified for each CD8 T cell cluster and highlighted on tSNE visualization (E).

https://doi.org/10.1371/journal.ppat.1012095.g003

response to infection, PEP-619WW mice have more effector-like CD4 T cells (cluster 1 and 4) as compared to PEP-WT mice.

Prolonged type I IFN (IFN-I) during LCMV-cl13 infection is associated with viral persistence [26,74]. Therefore, we next wanted to know if CD4 T cells from PEP-WT and PEP-619WW had different IFN-induced gene signatures. Using our scRNAseq 10x genomics data we looked at the change of expression in various interferon stimulated genes (ISGs) in PEP-WT and PEP-619WW CD4 T cells. *Isg20*, *Oasl2*, *Ifi44*, *Isg15*, and *Ifi27l2a* all have a log2 fold change greater than 0, indicating higher relative expression in PEP-WT mice (Fig 3C), suggesting PEP-619WW CD4 T cells had reduced IFN-I signaling cells.

CD8 T cell transcriptional identity in infected PEP-WT and PEP-619WW mice

Reclustering of CD8 T cells also grouped the cells into 4 distinct cell populations (Fig 2H). In PEP-WT mice, there was a relatively even distribution of each CD8 T cell cluster. When comparing the proportion of each cluster amongst all CD8 T cells in PEP-619WW mice, 2 of the clusters stood out as interesting based on percent of total CD8 cells within each genotype. Cluster 1 appeared overrepresented in the PEP-619WW (43.77%) mice compared to PEP-WT (24.46%) whereas cluster 3 was less represented in PEP-619WW CD8 T cells (8.19%) compared to PEP-WT CD8 T cells (25.75%) (Fig 2H).

Using their distinct transcriptional signatures, we further analyzed the CD8 T cell clusters of interest. Genes associated with T effector cell phenotype, *Gzma*, *Ccr2*, *Il18rap*, *Ahnak*, *Cxcr6*, and *Ifngr1* are upregulated in cluster 1 (Fig 3D) [38,74,76]. Additionally, using iPathway, the top three pathways associated with cluster 1 are viral protein interaction with cytokine and cytokine receptor, cytokine-cytokine receptor interaction, and cell adhesion molecules (Table 1). These pathways are associated in actively responding CD8 T cells. PEP-619WW

Table 1. Top Pathways upregulated within each CD8 T cell cluster of LCMV-13 infected mice at 8dpi. Gene expression data exported from Loupe for each CD8 T cell cluster, as identified in Fig 2, was uploaded to iPathway analysis to determine pathways which were significantly associated with those gene sets. Table shows the top 3 pathways for each indicated cluster, the count of differentially expressed (DE) genes that were expressed in each cluster associated with the pathways, count all genes in that pathway, and the p-value associating that pathway with the gene expression data set.

Cluster	Pathway Name	CountDE genes	CountALL genes	pValue
1	Viral protein interaction with cytokine and cytokine receptor	6	10	0.00014
	Cytokine-cytokine receptor interaction	8	16	0.00036
	Cell adhesion molecules	7	14	0.0026
2	Cell cycle	10	15	0.00022
	p53 signaling pathway	9	11	0.0013
	Apoptosis	14	22	0.0030
3	Cytokine-cytokine receptor interaction	8	16	2.55E-06
	Neuroactive ligand-receptor interaction	2	3	0.00026
	FoxO signaling pathway	6	9	0.00043
4	Pyrimidine metabolism	5	8	0.0012
	Gap junction	4	6	0.0049
	Small cell lung cancer	3	9	0.013

https://doi.org/10.1371/journal.ppat.1012095.t001

mice had a higher proportion of cluster 1 cells amongst total CD8 T cells compared to PEP-WT mice, suggesting PEP-619WW mice had more anti-viral effector CD8 T cells.

Cluster 3, which was proportionally more represented in PEP-WT mice, has numerous genes associated with either naïve CD8 T cells, memory CD8 T cells, and the transition from effector to memory cells (Fig 3D). These include *Il7r*, *Ccr7*, *Sell*, *Lef1*, and *Tcf7* [38,74–77]. Additionally, *Tcf7*, *Il7r* and *Bcl2* have been implicated in the memory/T cell exhaustion precursor cell population [74,76]. If cluster 3 was largely composed of activated effector cells, we would expect high expression of *Cd69* along with *Gzmb* (Fig 3E). *Cd69* is most highly expressed in cluster 3, indicating that this group is largely comprised of antigen experienced T cells. However, cluster 3 had the lowest expression of *Gzmb*, suggesting these cells are not functionally active. Pathways significant in cluster 3 are cytokine-cytokine receptor interaction, neuroactive ligand-receptor interaction, and the FoxO signaling pathway (Table 1). FoxO signaling is known to restrict T cell effector programs and terminal differentiation following LCMV infection [78]. Taken together, the expression of *Tcf7*, *Il7r*, and *Bcl2*, along with expression of *Cd69*, and FoxO signaling suggests that CD8 T cell cluster 3 contains pre-exhausted T cells. Infected PEP-WT animals had a higher proportion of cluster 3 among the total CD8 T cells compared to PEP-619WW mice.

Not all CD8 T cell clusters had a clear identity based on their transcriptional signatures. Interrogating the cluster 2 genes and pathway analysis we found these cells did not have an obvious functional phenotype but clearly were active. Some top genes in CD8 T cell cluster 2 are *Pclaf*, *Birc5*, and *Cdca8*. These genes are associated with formation of memory, anti-apoptotic pathways, and cell division [46,59]. The top pathways associated with cluster 2 is p53 signaling pathway, apoptosis, and cytokine-cytokine receptor interaction (Table 1). Within CD8 T cell cluster 4, some of the top genes are associated with the exhausted T cell progenitor pool such as *Slamf6*, *Tcf7*, and *Pou2f2* (Fig 3D) [79]. Surprisingly, antigen presentation genes, including *H2-Eb1*, *H2-Ab1*, and *H2-Aa* are also expressed in this cluster. To further confirm that cluster 4 is composed of CD8 T cells, we looked at the relative expression of *Cd3e* and *Cd8b1* in each CD8 T cell cluster (S1A–S1C Fig). All 4 clusters express these CD8 T cell markers. We also confirmed expression of the class II genes (S1D–S1F Fig). To determine if there were antigen presenting cells (APCs) contaminating our reclustered CD8 T cell population, we also looked at the expression of myeloid and B cell markers, *Lyz2*, *Csfr1*, and *Cd19*. Although there was no expression of *Cd19* in our CD8 T cell cluster, some cells in cluster 4 did express of *Lyz2* and *Csf1r*. The same cells also express *Cd3e* and *Cd8b1*. Importantly, expression of class II genes does overlap with that of *Lyz2* and *Csf1r*. Although class II expression in human T cells has been reported during Hepatitis C Virus (HCV), HIV-1, Ebola Virus, Dengue Virus, and SARS-CoV2 infections in humans, there is not strong evidence for this same observation in mice [80–85]. Pathways that connected with CD8 T cell cluster 4 are pyrimidine metabolism ($p = 0.001$), gap junction ($p = 0.004$), and small cell lung cancer ($p = 0.0133$) (Table 1). From this data we are unsure as to the identity of this cell population and future studies are needed to determine if class II gene expression in mice during virus infection is biologically relevant or if this is a transcriptional artifact in our study.

Pro-autoimmune allele enhances antigen specific T cell activation

Anti-viral CD4 T cell function. We next wanted to confirm that the transcriptional difference identified by scRNA-seq resulted in differences in protein expression and T cell function following infection. Th1 polarized CD4 T cells express high levels of the transcription factor Tbet and are a major source of IFNγ during viral infection, a cytokine critical for activating innate and adaptive immunity to clear a virus infection [35,85]. Following infection, PEP-

619WW had a higher frequency of Th1 cells, determined by CD44 and Tbet positive cells (Fig 4A and 4B). We next measured the amount of Tbet in the Th1 population in PEP-WT and PEP-619WW mice. As anticipated, Tbet expression was highest in Th1 cells from PEP-619WW mice 8 dpi (Fig 4C). Although there is a higher proportion of Th1 cells, it is possible that the functions of these T cell could be tempered by the presence of Tregs. However, examination of the proportion of Foxp3 expressing CD4 cells in LCMV infected animals showed that both genotypes exhibited a decrease in Tregs following infection (Fig 4D).

To directly test CD4 T cell anti-viral function, whole splenocytes were stimulated with the LCMV CD4 T cell immunodominant epitope peptide (GP_{61-80}) at 8 dpi. In this system, the antigen specific activation of the CD4 T cells reflects their function *in vivo*. A higher proportion of PEP-619WW CD44+ CD4 T cells produced IFNγ in response to stimulation when compared to the cells from PEP-WT infected mice (Fig 4F and 4G). Also, individual cells from infected PEP-619WW mice had a higher level of IFNγ production (Fig 4H). Furthermore, following peptide stimulation, PEP-619WW mice had a higher proportion of polyfunctional CD4 T cells, producing both IFNγ and IL-2 (Fig 4I). These data demonstrate PEP-619WW mice have a more activated and functional Th1 CD4 T cell population than PEP-WT mice at 8dpi.

Another key function of CD4 T cells during viral infection is differentiation into T_{FH} cells and development of antibody producing B cells in germinal centers, thus contributing to long lasting memory against the viral infection [86]. Of note, PEP-619WW mice exhibited almost twice the frequency of T_{FH} cells among CD4 T cells, as early as 8 days post infection (Fig 4E). This coincided with increased serum titer of anti-LCMV IgG2A antibody in PEP-619WW mice 9 dpi (S2 Fig).

Antiviral CD8 T cell function. CD8 T cell function is also required for clearance of LCMV-cl13 [21]. Based on the scRNAseq data and increased function of anti-viral CD4 T cells, we hypothesized that we would see increased CD8 T cell activation and anti-viral function. At 8 dpi, we did not detect a difference in the proportion of activated CD8 T cells between PEP-WT and PEP-619WW mice, as measured by CD44 (Fig 5A). However, when we interrogated these activated CD8 T cells for expression of effector molecules, we did observe an increase in expression in CD107a on CD44+ CD8 T cells from infected PEP-619WW mice compared to infected PEP-WT mice (Fig 5B). Further, these cells had increased in perforin expression (Fig 5C). We also observe a slight increase in the frequency of immunodominant epitope, GP_{33-41} (GP33), specific CD8 T cells (Fig 5D) in infected PEP-619WW mice, compared to infected PEP-WT mice. However, the absolute cell number was not different between genotypes (Fig 5E). When spleen from 8-day infected mice were stimulated with the CD8 T cell immunodominant epitope, GP33, we did not detect any difference in IFNγ production between the two genotypes (Fig 5F and 5G). These data suggest that at 8 dpi, while activated PEP-619WW CD8 T cells have increased expression of some effector molecules, PEP-619WW does not have a significant impact on CD8 T cell IFNγ production against the immunodominant epitope of LCMV-cl13.

PEP-619WW mice have a more immunostimulatory DC phenotype during chronic viral infection

The myeloid compartment contains numerous subsets that may contribute to viral clearance and enhanced CD4 T cell function as observed in PEP-619WW infected mice [25,31–34,88]. Classical dendritic cells (cDCs, CD11c+ MHCII+) are critical APCs during viral infection [34]. It is well established that expression of inhibitory ligand PD-L1 suppresses T cell function during LCMV infection [88]. At 8 dpi there is a significant decrease in proportion of splenic

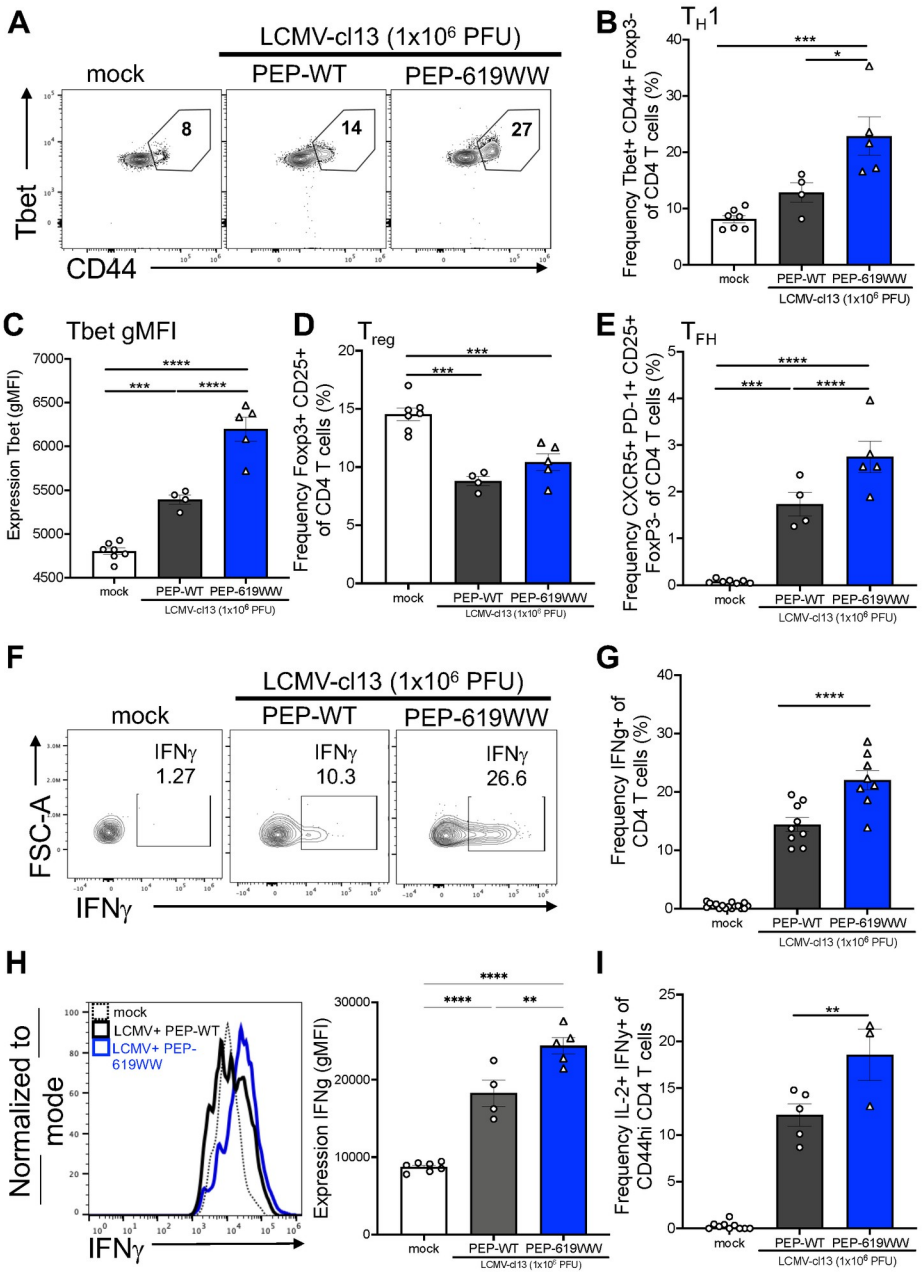

Fig 4. PEP-619WW mice have enhanced CD4 T cell activation during LCMV-cl13 infection. 8dpi splenocytes were isolated and examined for CD4 T cell subsets. Th1 cell (Lymphocytes> single cells x2> live> CD3+ Cd19-> CD4 + CD8α-> Foxp3- CD44+> Tbet+) representative flow plot (A), Th1 frequency of total CD4 (B), and gMFI of Tbet in CD44+ CD4 T cells (C) in mock infected (white bar, circles), infected PEP-WT (black bar, circles), and infected PEP-619WW (blue bar, circles). Frequency of Tregs amongst total CD4 T cells (Lymphocytes> single cells x2> Live> CD19- CD3+> CD4+ CD8α-> Foxp3+ CD25+) (D). Frequency T_{FH} cells (Lymphocytes> single cells x2> Live> CD19- CD3+> CD4+ CD8α-> Foxp3- CD25+> CXCR5+ PD-1+) (E). CD4 T cells were also assessed for IFNγ and IL-2 production after peptide (GP_{61-80}) stimulation (F,G,H). IFNγ+ cells representative flow plot (F). IFNγ+ of CD44 + CD4+ T cells (Lymphocytes> single cells x2> live> CD3+ Cd19-> CD4+ CD8α-> CD44+ >IFNγ+) quantification (G). Expression of IFNγ in CD44+ CD4+ T cells, representative histogram (H) and quantification (H). Frequency of IL-2+ IFNγ+ CD44hi CD4+ T cells (Lymphocytes> single cells x2> live> CD3+ Cd19-> CD4+ CD8α-> CD44+ >IFNγ+ IL-2+). Representative experiment or sample shown for A-F, H-I. Pooled data in G. Each dot represents an individual mouse. Experiments were repeated at least 3 times. SEM shown. *p<0.05, **p<0.01, ***p<0.001, ****p<0.0001. One Way ANOVA with Tukey Post Hoc Analysis.

https://doi.org/10.1371/journal.ppat.1012095.g004

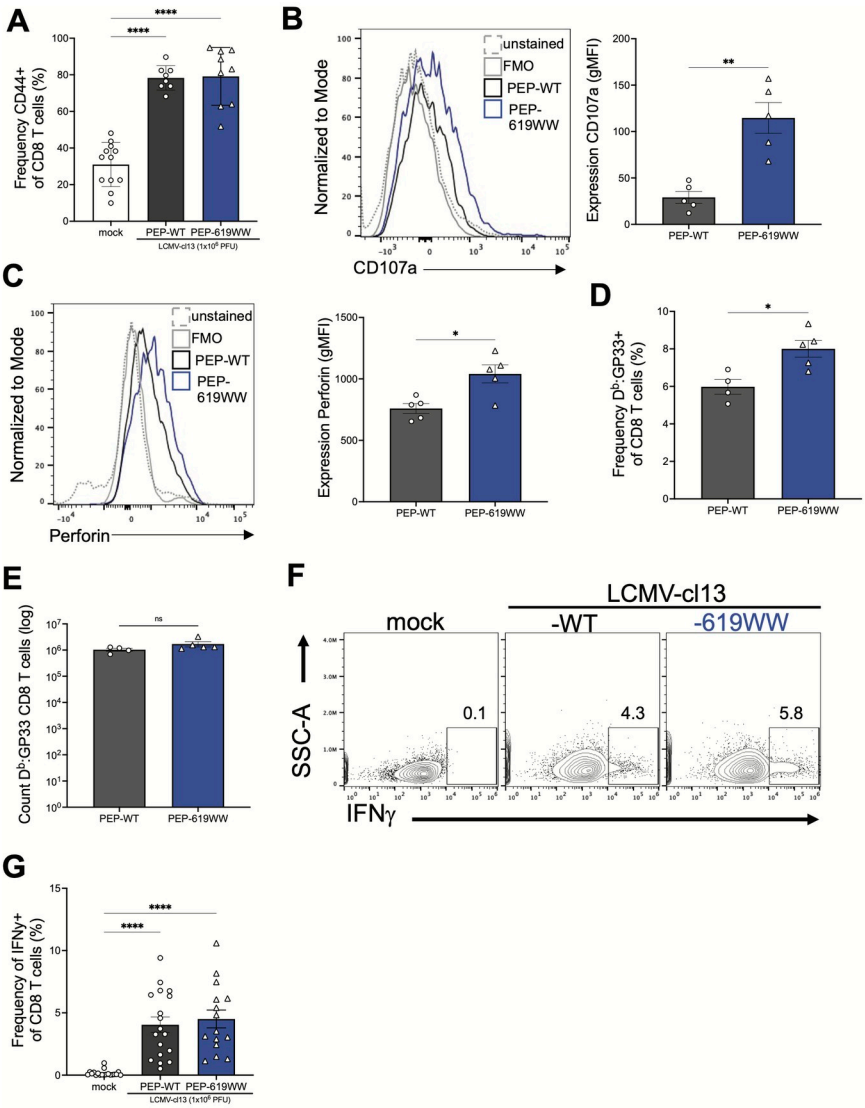

Fig 5. PEP-619WW and PEP-WT mice have comparable function against the LCMV immunodominant epitope GP_{33-41}. 8dpi splenocytes from mock infected (white), PEP-WT (black), and PEP-619WW (blue) were isolated and examined for virus specific CD8 T cell subset, assess CD8 T cell activation and function against GP_{33-41}. Frequency of activated CD8 T cells (Lymphocytes> single cells x2> live> CD3+ Cd19-> CD4- CD8α+> CD44+) (A). Expression of degranulation marker CD017a on activated CD8 T cells (CD44+ CD8 T cells) (representative histogram [left] and gMFI quantification [right] (B). Expression of perforin in activated CD8 T cells (CD44+ CD8 T cells) (representative histogram [left] and gMFI quantification [right] (C). Frequency of Db:GP33 tetramer+ CD8 T cells (Lymphocytes> single cells x2> live> CD3+ Cd19-> CD4- CD8α+> Db:GP33+) (D), and absolute number of Db:GP33 CD8 T cells (E). Whole splenocytes were stimulated with GP_{33-41} peptide. Representative flow plots showing IFNγ production in response to GP33 peptide (F) and quantification (G). Data in G is pooled from multiple experiments. All other data is from a representative experiment. SEM shown. *p<0.05, **p<0.01, ***p<0.001, ****p<0.0001. One Way ANOVA with Tukey Post Hoc Analysis. Experiments repeated 3 independent times. Individual data points represent a single animal.

https://doi.org/10.1371/journal.ppat.1012095.g005

PD-L1+ cDCs in PEP-619WW mice (Fig 6A and 6B). Furthermore, PD-L1 expression was lower on PEP-619WW cDCs (Fig 6C and 6D).

Given the diversity of cDC subsets in the spleen, we addressed whether a specific cDC subset had decreased PD-L1 expression or if all DC subsets were affected comparably at 8 dpi.

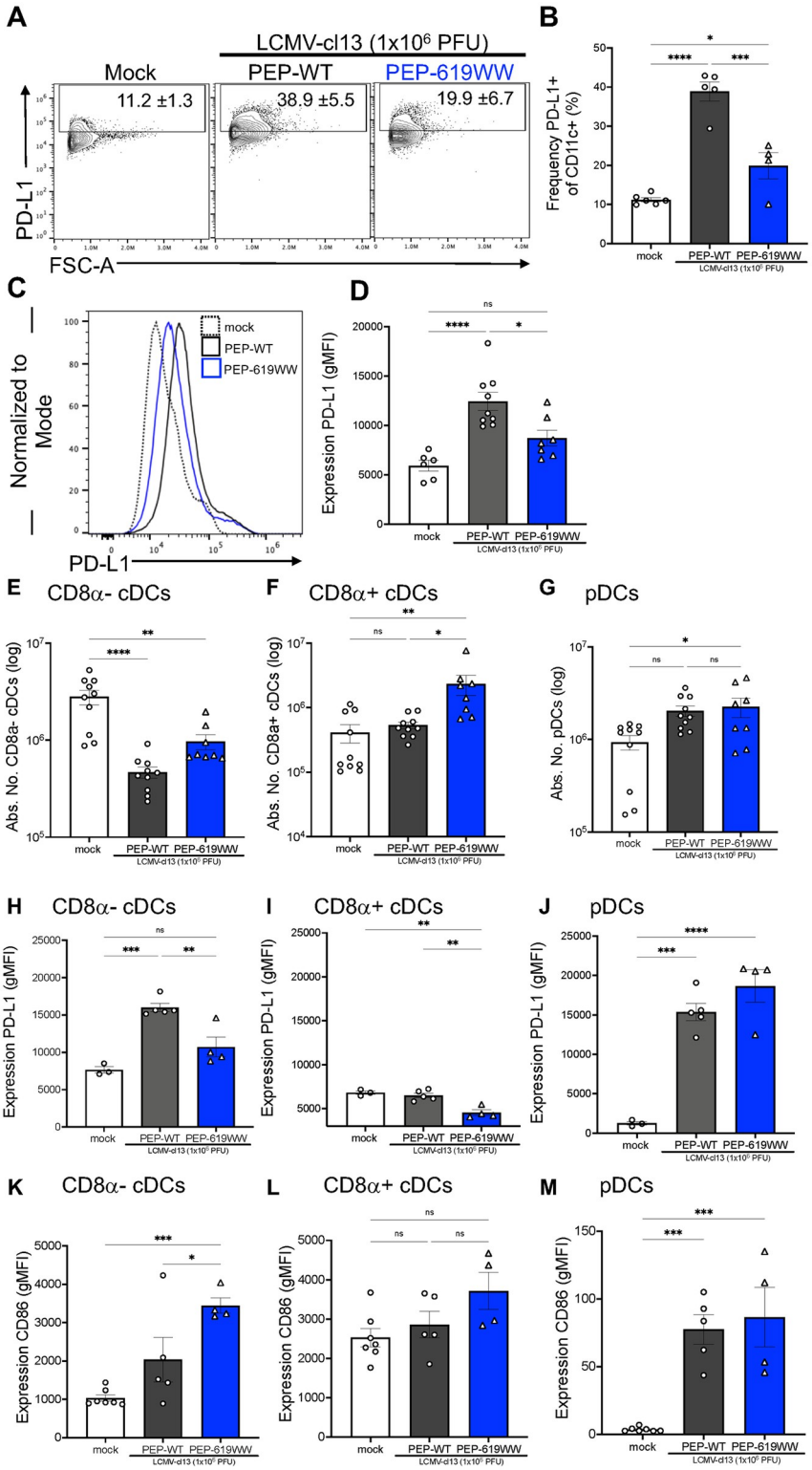

Fig 6. *Ptpn22* pro-autoimmune allele promotes more immunostimulatory-like CD8α- cDCs during LCMV-cl13 infection. 8dpi spleens were harvested from mock infected (white, circle), infected PEP-WT (black, circles), and infected PEP-619WW (blue, triangles) mice. Representative flow plot (A) and quantification (B) of PD-L1+ among CD11c+ cells (Lymphocytes> Single cell x2> Live> CD3- CD19-> Ly6G- CD11b+/->CD11c+ F4/80-). PD-L1 expression on CD11c+ cells representative histogram (C) and quantification (D). Absolute number of CD8α- cDCs

(Lymphocytes> Single cell x2> Live> CD3- CD19-> Ly6G- CD11b+/->CD11c+ F4/80->CD8α- PDCA-1->MHC-II (I-Ab)+) (E), CD8α+ cDCs (Lymphocytes> Single cell x2> Live> CD3- CD19-> Ly6G- CD11b+/->CD11c+ F4/80->CD8α+ PDCA-1->MHC-II (I-Ab)+) (F), and pDCs ((Lymphocytes> Single cell x2> Live> CD3- CD19-> Ly6G- CD11b+/->CD11c+ F4/80->CD8α+/- PDCA-1+> Ly6C+ B220+) (G). Expression (gMFI) of PD-L1 on CD8α- cDCs (H), CD8α+ cDCs (I) and pDC (J). Expression (gMFI) of CD86 on CD8α- cDCs (K), CD8α+ cDCs (L), and pDCs (M). Representative experiment or sample shown. Each dot represents an individual mouse. Experiments were repeated at least 3 times. SEM shown. ns = not significant $^{*}p<0.05$, $^{**}p<0.01$, $^{***}p<0.001$, $^{****}p<0.0001$. One Way ANOVA with Tukey Post Hoc Analysis.

https://doi.org/10.1371/journal.ppat.1012095.g006

First, we assessed the numbers of different major DC subsets present in PEP-WT and PEP-619WW mice. It has been shown that following LCMV-cl13 infection, there is a significant drop in numbers of cDCs present in the spleen [34,90]. Indeed, both PEP-WT and PEP-619WW mice showed a significant decrease in the numbers of $CD8\alpha^{-}$ cDCs (CD8α- CD11b + PDCA-1- CD11c+ DCs) (Fig 6E). However, PEP-619WW mice had significantly more $CD8\alpha^{+}$ cDCs (CD8α+ CD11b- PDCA-1- CD11c+ DCs) at 8dpi compared to PEP-WT mice (Fig 6F). We also looked at plasmacytoid DCs (pDCs) as they are known for their role in supporting clearance of LCMV-cl13 infection [90]. PEP-619WW mice had more pDCs (PDCA-1 + B220+ Ly6C+ CD8α- CD11c+/- DCs) following infection, compared to mock infected animals (Fig 6G). We did not detect a difference in the number of pDCs between mock and infected PEP-WT mice (Fig 6G).

We next examined levels of PD-L1 expression on these same DC subsets at 8dpi. $CD8\alpha^{-}$ cDCs, but not $CD8\alpha^{+}$ cDCs, upregulate PD-L1 in infected PEP-WT mice (Fig 6H, 6I and 6J). PEP-619WW $CD8\alpha^{-}$ cDCs have less PD-L1 expression than PEP-WT $CD8\alpha^{-}$ cDCs at 8dpi (Fig 6H). Also, PEP-619WW $CD8\alpha^{+}$ cDCs have less PD-L1 expression compared to infected PEP-WT mice and mock-infected animals. pDCs from both PEP-WT and PEP-619WW have significantly higher levels of PD-L1 compared to uninfected controls (Fig 6J). We also looked at CD86 expression, a receptor that positively regulates T cell activation by DCs. CD86 expression was increased in $CD8\alpha^{-}$ and pDCs in both PEP-WT and PEP-619WW mice following infection. However, the level of increase was significantly greater on $CD8\alpha^{-}$ cDCs from PEP-619WW mice (Fig 6K–6M). Thus, infected PEP-619WW mice have cDC populations with lower PD-L1 expression and enhanced CD86 expression, suggesting a more immunostimulatory phenotype.

Ptpn22 pro-autoimmune allele enhances T cell activation through T cell intrinsic and extrinsic mechanisms

We next wanted to know if the enhanced anti-viral CD4 T cell function observed was due to a T cell intrinsic mechanism, such as enhanced TCR signaling, or a T cell extrinsic mechanism, such as a more immunostimulatory cDC phenotype. Employing adoptive transfer techniques, we constructed mice in which the virus specific CD4 T cells (SMARTA CD4 T cells) expressed an allelic difference in *Ptpn22* (Fig 7A). Post infection, both transferred SMARTA PEP-WT and SMARTA PEP-619WW CD4 T cells expanded, regardless of host genotype (Fig 7B and 7C). In the PEP-WT host, SMARTA PEP-619WW CD4 T cells had a higher proportion of IFNγ+ cells than SMARTA PEP-WT CD4 T cells (Fig 7D and 7E). When SMARTA PEP-WT CD4 T cells were transferred into a PEP-619WW host, there was a slight increase in the proportion of IFNγ+ virus specific CD4 T cells compared to SMARTA PEP-WT T cells into a PEP-WT host (Fig 7D and 7E). However, SMARTA PEP-619WW CD4 T cells in a PEP-619WW host had the highest frequency of IFNγ+ virus specific cells (Fig 7D and 7E). Additionally, SMARTA PEP-619WW cells in a PEP-619WW had the highest expression of IFNγ

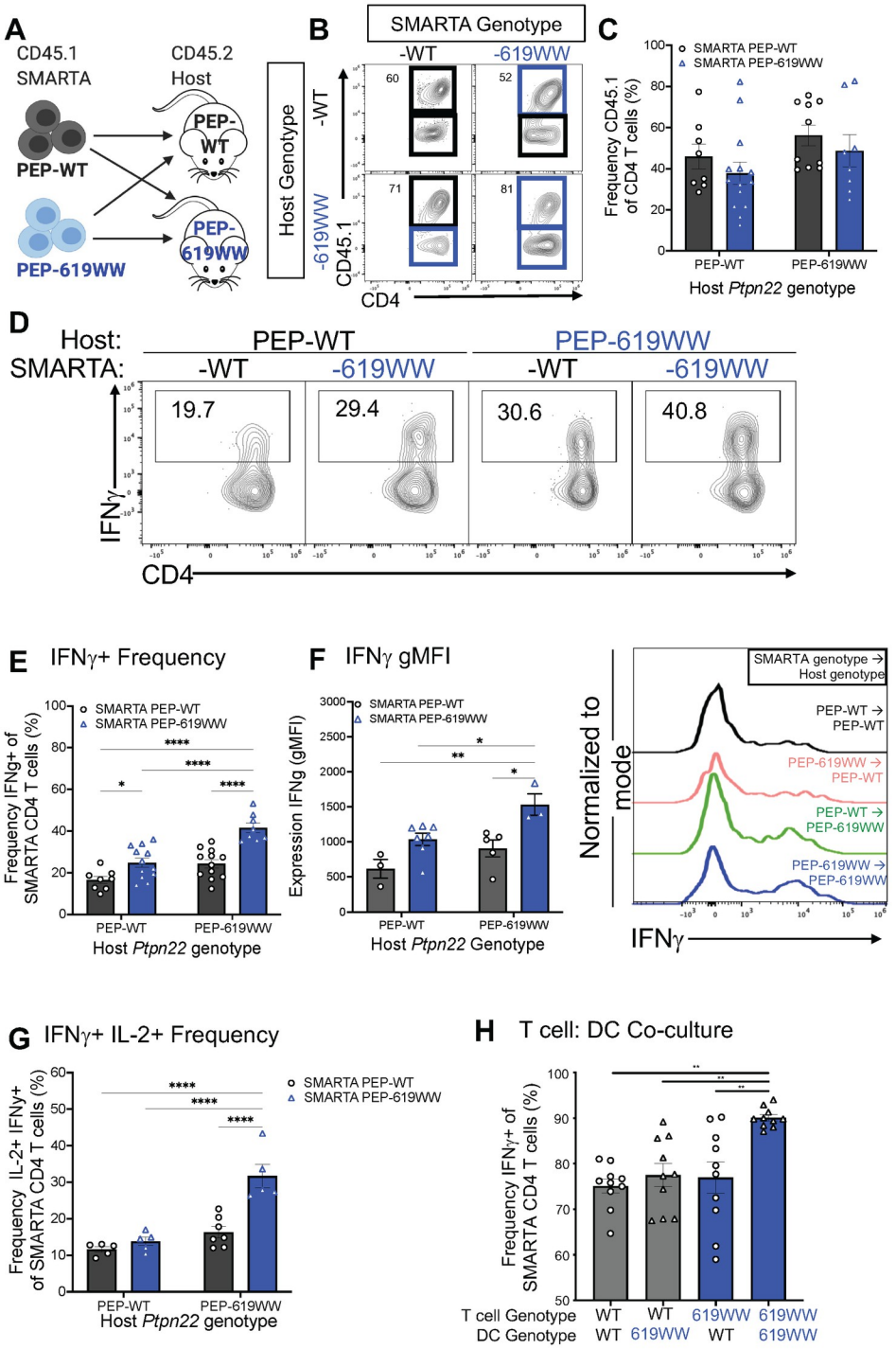

Fig 7. *Ptpn22* alternative allele enhances anti-viral T cell activation through T cell intrinsic and T cell extrinsic mechanisms. CD45.2 C57BL/6 mice (PEP-WT or PEP-619WW) received 5x10^4 CD45.1 SMARTA CD4 T cells prior to being infected with LCMV-cl13 (diagram created with biorender.com) (A). Frequency of CD45.1 SMARTA T cells (Lymphocytes> single cells x2> Live> CD3+ CD19-> CD4+ CD8α-> CD44+> CD45.1+ CD45.2-) for each transfer condition, representative flow plot (B) and quantified (C). Following peptide stimulation with $GP_{61\text{-}80}$ peptide, IFNγ and IL-2 production of SMARTA cells were measured (D-G). Representative flow plot showing IFNγ+ CD45.1+ CD4 T cells (D), quantification IFNγ+ CD45.1 Cd4 T cells (E), expression (gMFI) of IFNγ in CD45.1 SMARTA cells with representative histogram (F), frequency of IFNγ+ IL-2+ CD45.1 CD4 T cells (G). PEP-WT or PEP-619WW FLT3L-differentiated DCs were pulsed with $GP_{61\text{-}80}$ peptide then incubated with PEP-WT or PEP-619WW SMARTA CD4 T cells for 3 days. Following incubation, SMARTA T cell function was determined through IFNγ production by

intracellular cytokine staining and measured on a flow cytometer (H). C, E, G, and H from pooled data. F is a representative experiment. Experiments were repeated at least 3 times. SEM shown. $^{*}p<0.05$, $^{**}p<0.01$, $^{***}p<0.001$, $^{****}p<0.0001$, Two Way ANOVA with Sidak post hoc analysis.

https://doi.org/10.1371/journal.ppat.1012095.g007

+ within activated CD4 T cells (Fig 7F). Also, SMARTA PEP-619WW CD4 T cells in a PEP-619WW host had the highest proportion of polyfunctional cells (Fig 7G). To test this further, we co-cultured peptide-pulsed, FLT3L differentiated PEP-WT or PEP-619WW dendritic cells (DCs) with PEP-WT or PEP-619WW SMARTA CD4 T cells (Fig 7H). Only when PEP-619WW was present in both DCs and CD4 T cells was there the most IFNγ production (Fig 7H). Taken together, this suggests the presence of the *Ptpn22* minor allele in either the host or SMARTA CD4 T cells slightly increased T cell function. However, the T cell intrinsic and T cell extrinsic effects have an additive effect on virus specific T cell activation, resulting in the highest amount of IFNγ and IL-2 production.

Discussion

The strong genetic link between the *PTPN22* minor allele (R620W) and autoimmunity would be expected to be an evolutionary disadvantage [7]. However, an advantage in eradicating pathogens could help explain why the variant persists in the population [91,93]. Thus, it was of interest to assess the impact of the *PTPN22* autoimmunity associated allele has during virus infection. Previously, using mice deficient in *Ptpn22* expression (PEP-null), we demonstrated that *Ptpn22* promotes T cell exhaustion, thus permitting LCMV-cl13 persistence [27]. Although some studies have found that the lack of *Ptpn22* is similar in phenotype to R620W (R619W in mice) several differences have also emerged. This may be because the 620W (619W) variant does not directly affect the phosphatase activity of this enzyme [14,94,95]. Rather, the presence of tryptophan disrupts the ability of the enzyme to bind with other proteins such as CSK and TRAF3 [13,15,95]. As an example of differing consequences, whereas PEP-null mice exhibit an increased frequency and potency of Tregs as compared with WT [96], this same Treg phenotype is not observed in naïve mice bearing the *Ptpn22* pro-autoimmune allele [18,97]. Despite its importance in human health, studies have not investigated whether the *Ptpn22* autoimmunity associated minor allele impact anti-viral immune responses.

Using the well-established model of LCMV-cl13, we tested the ability PEP-619WW mice to overcome a potentially chronic viral infection. PEP-619WW mice largely cleared virus infection and have reduced weight loss compared to wildtype (PEP-WT) mice (Fig 1A–1D). Considering comparable LCMV-NP expression at 3 dpi, our data suggests that clearance is not likely due to early changes in tropism (Fig 1E). By day 8 PEP-619WW demonstrated earlier viral clearance in monocytes, marginal zone macrophages, and pDCs, but this does not correlate with reduced sera titer (Fig 1F). Future studies will address the mechanism(s) in PEP-619WW mice driving viral clearance from these myeloid subsets. Taken together, these data demonstrate expression of PEP-619WW, rather than the WT allele, confers strong protection from virus persistence.

Failure to clear LCMV-cl13 infection is associated with immune cell dysfunction [26,26,34,74,98]. The use of scRNAseq allowed us to transcriptionally define and interrogate multiple immune cell types in both PEP-WT and PEP-619WW mice during LCMV-cl13 infection (Fig 2). These data suggest the impact of PEP-619WW during viral infection is pleiotropic and impacts multiple mechanisms that result in altered B cell, myeloid cell, and T cell

responses. The details of how PEP-619WW impacts different molecular mechanisms within each cell during virus infection is of ongoing interest.

Both CD4 and CD8 T cells are necessary to clear LCMV-cl13 [26]. We investigated the T cell compartment from infected PEP WT and PEP-619WW mice at a transcriptional and functional level. Anti-viral CD4 T cells, but not CD8 T cells, were functionally different in infected PEP-619WW mice. Among CD4 T cells, PEP-619WW mice had higher frequencies of T_{FH} and activated/effector-type CD4 T cells during infection than PEP-WT animals (Figs 3A and 4E). During chronic viral infection, sustained TCR signaling is shown to lead to more T_{FH} cell differentiation compared to acute viral infection [98]. Since *Ptpn22* tempers TCR signaling, disrupting that regulatory mechanism, through presence of the allelic variant (PEP-619WW) may be what is driving this T_{FH} increase during infection. It has been shown that *Ptpn22* pro-autoimmune allele bearing mice and *Ptpn22* knock out mice have increased T_{FH} and germinal center formation [96,99]. We also show that transcriptionally and functionally, PEP-619WW have more activated and anti-viral effector CD4 T cells. CD4 T cells from PEP-619WW infected mice produced more IFNγ, and IL-2 compared to PEP-WT cells (Fig 4F–4I). Presence of these polyfunctional cells has been linked to be better anti-viral immune response. Taken together, our data demonstrate PEP-619WW have enhanced anti-viral CD4 T cell responses.

Both T cell intrinsic and T cell extrinsic mechanisms could explain the enhanced anti-viral CD4 T cell function in PEP-619WW mice. Modifying TCR strength through extrinsic signals, such as increased immunostimulatory molecules, or intrinsic signals have an impact on downstream effector functions like IFNγ production [100,101]. Using murine models, human T cell culture systems, and clinical data researchers have defined a role of *PTPN22/Ptpn22* in tempering the TCR signaling pathway. In these systems, researchers have also shown that the pro-autoimmune allele of *PTPN22* results in sustained TCR signaling, leading to increased T cell activation [14,94]. Using adoptive transfers studies, we concluded that neither a PEP-619WW T cell nor host alone is sufficient to account for the heightened antigen-specific T cell activation during LCMV-cl13 infection. Rather, there is an additive effect between the antigen-specific PEP-619WW T cell, and PEP-619WW environment resulting in increased CD4 T cell activation. Taken together with our cDC profiling data and *ex vivo* co-culture data, it is likely that the large increase of CD4 T cell activation during LCMV-cl13 infection is from additive effects of the $CD8\alpha^-$ cDC being a more activator-like phenotype and the CD4 T cell having intrinsic properties to increase T cell activation. However, this does not rule out other cells, such as the NK cell or macrophage, in contributing to increased antigen-specific CD4 T cell function in PEP-619WW mice.

Our data suggest that the presence of the *Ptpn22* autoimmunity associated allele affects multiple parts of the anti-viral immune response critical for controlling a chronic infection. When the PEP-619WW cDCs prime and activate CD4 T cells, the T cells are interacting with a cDC that expresses less PD-L1 and increased CD86, in turn resulting in more T cell activation. PEP-619WW bearing T cells also demonstrate enhanced T cell intrinsic activation and production of IFNγ, potentially through the decreased tempering of TCR signaling or changed IFN-I signaling [14,94,102]. The PEP-619WW DC and PEP-619WW CD4 T cell have an additive effect on anti-viral T cell function, which in turn controls the chronic viral infection. Although we did not observe increased numbers of GP_{33}-specific CD8 T cells, these data do not rule out the possibility CD8 T cells against other epitopes contribute to viral clearance in PEP-619WW mice. Additional studies isolating the cell autonomous impact of PEP-619WW are needed to determine which cell type is necessary and/or sufficient to cause enhanced anti-viral T cell function and an enhanced anti-viral immune response. Results of this study provide a platform to further investigate the inter-relationships between immune cells to achieve a

desired phenotype as well as determine if/how other autoimmunity associated alleles affect the anti-viral immune response.

Methods

Ethics statement

All animal studies were reviewed and approved by Scripps Research Institutional Animal Care and Use Committee (IACUC) (protocol number: 06–0291) and University of Kansas (IACUC) (protocol number: 278–01).

Mice

Both males and females ranging from 6–12 weeks of age were used in this study. Animals were housed in general housing conditions at Scripps Research. We do not observe any sex-based difference in these studies with our animals. All animal studies were reviewed and approved by Scripps Research Institutional Animal Care and Use Committee (protocol number: 06–0291). C57BL/6 WT mice were originally purchased from Jackson labs, and then bred and maintained in Scripps Animal Facility. *Ptpn22* R619W (PEP-619WW) mice were generated using CRISPR/Cas9 technology on a C57BL/6 background using methods previously reported [97,103] in the Mowen Lab. In short, four nucleotides were replaced on exon 14 of *Ptpn22* to insert the BspEI restriction site and cause an arginine (R) to tryptophan (W) amino acid substitution at amino acid position 619. Genotypes were confirmed through PCR using the following primers which flank the mutated region of *Ptpn22*: Forward-5' AGCTGATGAAAATGTCCTATTGTGA 3' and Reverse-5' GTCCCACTGCATTCTGGTGA 3'. After amplification, PCR products are digested overnight at 37˚C with the restriction enzyme, BspEI, which is unique to mutated mice. Digested PCR products are run on a 2% agarose gel to visualize digested bands.

For transfer experiments, naïve CD4 T cells were isolated from the spleens of naïve CD45.1 SMARTA PEP-WT, PEP-null, or PEP-619WW C57BL/6 mice using a naïve CD4 negative isolation kit following manufacturer's specifications (Stem Cell Technologies, Vancouver, British Columbia, Canada). Cells were greater than 95% pure, as measured by flow cytometry. A low number of isolated CD4 T cells, as indicated in figure legend, were transferred into naïve, sex-matched mice intravenously. 1–2 days following cell transfer, recipient mice were infected with LCMV-cl13, or sterile HBSS for mock control.

For infection, mice received $1x10^6$ PFU LCMV-cl13 resuspended in 100uL sterile PBS intravenously (i.v). Mice receiving mock infection received 100uL sterile PBS (i.v). Mock group of mice included both PEP-WT and PEP-619WW genotypes. Mice were removed from study if weight loss was greater than 25% original starting weight.

Flow cytometry and antibodies

Samples were excised and placed into HBSS with 2% FBS. Samples were minced and incubated with Stem Cell Spleen dissociation media (Stem Cell Technologies, Vancouver, British Columbia, Canada) according to manufacturer's instructions. Following incubation, minced sample was smashed and filtered through 40uM filter to create a single cell suspension. Single cell suspension was counted and resuspended to desired concentration (dependent on experiment) in HBSS with 2% FBS. Single cell suspensions were used for staining and flow cytometric analysis. Cells were stained in serum free HBSS.

All flow cytometry was completed on a spectral cytometer the Cytek Aurora with a 4 laser or 5 laser system (405nm, 488nm, 640nm, 561nm, and 355nm (5 laser only)). Single color

stain OneComp eBeads (Thermo Fisher) were used for unmixing. Unmixed files were analyzed using FlowJo Software (BD Biosciences, San Diego, California). Antibodies used in various combinations (depending on experiment) are as follows: Ghost Viability Dye (v510, Tonbo Biosciences, 1:1000 dilution), CD3e (PE-Cy5/AF532, Tonbo Bioscience/Thermo Fischer, 1:200, clone 145-2C11), CD4 (PerCP/BV605, Tonbo Bioscience/Biolegend, 1:200, clone RM4-5), CD8α (APC-Cy7/APC-H7/APC, BD Biosciences, 1:200, clone 53–6.7), CD11c (PE-Cy5.5, Thermo Fisher, 1:100, clone N418), CD11b (PerCP-Cy5.5, Biolegend, 1:200, clone M1/70), F4/80 (Pacific Orange, Thermo Fisher, 1:100, clone BM8), IFNγ (AF647, Biolegend, 1:100, clone XMG1.2), TNFα (PE-Cy7, Beiolegend, 1:100, clone MP6-XT22), IL-2 (PE/BV421, Biolegend, 1:50, clone JES6-5H4), PDCA-1 (Pacific Blue, Biolegend, 1:200, clone 129C1), CD80 (BV421, 1:200, clone 16-10A1), CD86 (BV605, Biolegend, 1:200, clone GL1), PD-1 (PE-Cy7, Tonbo Biosciences, 1:200, clone J43.1), PD-L1 (PE/BV711, Tonbo Biosciences/Biolegend, 1:100, clone 10F.9G2), CD44 (AF700, Biolegend, 1:200, clone IM7), CD62L (FITC, Tonbo Biosciences, 1:100, MEL-14), Ly6C (BV785, Biolegend, 1:200, clone HK1.4), Ly6G (PE-eFlour610, Invitrogen, 1:200, clone IA8), CD206 (AF647, Biolegend, 1:100, clone CO68C2), CD209b (APC, Tonbo Biosciences, 1:200, clone 22D1), NK1.1 (FITC, Biolegend, 1:100, clone PK136), CD19 (BV711, Biolegend, 1:400, clone 6D5), B220 (APC-Cy5.5, Invitrogen, 1:200, clone RA3-6B2), MHC II I-Ab (FITC, Biolegend, 1:200, clone AF6-120.1), CXCR5 (BV605, Biolegend, 1:100, clone L138D7), Tbet (APC/AF647, Biolegend, 1:200), Foxp3 (PE, Invitrogen, 1:100, clone FJK-16s), LCMV-NP (self-conjugated to AF488 using Thermo Fisher AF488 labeling kit per manufacturer's instructions, BioXcell, 1:50, clone VL-4).

Tetramer staining occurred in the following conditions with HBSS. CD4 tetramer (I-Ab:GP66-77 (1,200)) was stained at 37C for 2 hours, in dark, alone. CD8 tetramer (D^b:GP_{33-41} (1,500)) was stained at room temperature, 1 hour, in dark, alone. Following tetramer stains, cell were washed and stained for other surface markers.

All non-tetramer surface markers were stained in HBSS, at 4C, in dark. If intracellular staining for transcription factors was required, Tonbo Foxp3 Fix/Perm kit was used per manufacturer's instructions. For intracellular cytokine staining BD Cytofix and Permwash was used according to manufacturer's instructions.

Representative gating strategy in S3 Fig.

Virus

LCMV-cl13 generation, tittering, and infection is as previously described [26,27,104]. In short, mice were infected with $1x10^6$ PFU LCMV-cl13. Throughout infection, mice were monitored and then euthanized at designated time points. To determine viral load in animals, serum and organs were harvested at designated time points and tittered on Vero cells and calculated as previously described [26].

Antigen-Specific T cell activation

Splenocytes from LCMV-cl13 or mock infected animals were isolated at designated time points. After red blood cell lysis and filtering through 70uM filter, splenocytes were resuspended in T stimulation media (RPMI containing 10% FBS, 1% of each of the following Penicillin/Streptomycin, HEPES, Sodium Pyruvate, L-Glutamine, Non-Essential Amino Acids, and 55μM 2-Mercaptoethanol). $2x10^6$ splenocytes were plated into 96-U bottom wells in the presence or absence of 5μg/mL GP_{61-80} peptide (CD4 T cells) or 2μg/mL $GP33_{61-80}$ (CD8 T cell) for 1 hour at 37C. After 1 hour incubation with peptide, Brefeldin A (0.4ug/mL) was added and incubated for an additional 4 hours at 37C. Following stimulation and incubation,

cell were spun down, washed with HBSS, and proceeded to extracellular and intracellular staining.

Bone marrow dendritic cells (BMDCs)

Bone marrow cells were isolated from PEP-WT and PEP-619WW mouse femurs. Additional experiments directly compared BMDCs from immune competent PEP-WT and PEP-619WW bone marrow cells and Rag1 -/- PEP-WT and Rag1-/- PEP-619WW and did not detect differences in their capacity to activated CD4 T cells. Following isolation, bone marrow cells were cultured in Advanced DMEM containing 10% FBS, 1% penicillin streptomycin, 1% L-Glutamine, and 100ng/mL FLT3L (Stem Cell Technologies, Vancouver, CA) for 8 days. On day 8, FLT3L-differentiated dendritic cells were harvested, counted, and re-plated for further assays.

T cell: DC co-culture

Naïve CD4 T cells were isolated from naïve SMARTA PEP-WT or PEP-619WW C57BL/6J mice using a negative selection kit (StemCell Technologies). Isolated T cells were incubated at a 3:1 (T cell: DC) ratio with FLT3L-differentiated peptide (GP_{61-80}) pulsed BMDCs for 3 days at 37 C. On day 3 of incubation, all cells were harvested to determine T cell activation and IFNγ production via intracellular cytokine staining and flow cytometry. Non-peptide pulsed FLT3L-differentiated cells were used as a negative control for T cell function and gating for flow cytometry.

Single cell RNA sequencing and analysis

At 8dpi, spleens from 4–5 age matched, sex matched PEP-WT and PEP-619WW mice were removed, processed (as described above), and resuspended in a single cell suspension. Splenocytes from each genotype were pooled and FACS sorted for Live CD45+ cells. Sorted cells were submitted to the Scripps Research Genome Sequencing Core for single cell RNA sequencing via 10x Genomics platform with the following details: Illumina Nextseq 2000 platform, Illumina flowcell P2 v3 100 cycles (400 mil reads), 10X protocol CG000315 Rev B, chemistry "Single Cell 3" v3.1, constructs with the following paired read structure: Read 1 length 28, Read 2 length 90, Indexing Read length 20, the target sequencing depth was 10,000 cells/ sample, 20,000 reads/cell, total: 400 million reads, 200 million for each sample.

The QC results were the following: sample 1 (PEP-WT) had 9, 539 estimated number of cells, 22, 358 mean reads per cell, and 1,709 median genes per cell while sample 2 (PEP-619WW) had 11, 029 estimated number of cells, 14,321 mean reads per cell, and 1,477 median genes per cell.

We performed primary and secondary analysis of scRNA-Seq data using CellRanger (Cellranger version 6.1.1 with 10X reference transcriptome "mm10-2020-A", for chemistry "Single Cell 3' v3"), an analysis suite consisting of multiple pipelines for end-to-end analysis of single cell data. It uses a custom-built wrapper around Illumina's bcl2fastq to demultiplex raw base calls. This is followed by removal of duplicates using UMI (unique molecular identifier) counting. These preprocessed samples are aligned using STAR [105], which performs splicing-aware alignment of reads to the genome. Aligned reads are then bucketed into exonic and intronic regions using a reference GTF (gene transfer format) file. Finally, read counts per gene are calculated, and these values are used for downstream estimation of differentially expressed genes. The unbiased single-cell profiles and high-resolution data allows counting and clustering of cells with similar transcriptome profiles to uncover distinct cell subsets and genes preferentially expressed by the cells. We performed dimensionality reduction, clustering, generation of open-standard file formats for interactive analysis, using both: currently most widely adopted

methods and algorithms [106–107] as well as most recent and better performing methods and algorithms [109–111] now available. We performed interactive exploration and functional analysis, to uncover cells sub-populations, gene markers and differential expression between sample groups, and suggest possible pathways and mechanisms, leveraging leading edge platforms for single cell exploration [112] and complex functional analysis [113].

Visualization, clustering, and population identification, and gene expression was all completed with Loupe Software. t-distributed stochastic neighbor embedding (tSNE) visualization and Uniform Manifold Approximation and Projection (UMAP) clustering were performed using aggregated file containing both PEP-WT and PEP-619WW samples. Data is shown using tSNE visualization.

Anti-LCMV neutralizing antibody assay

Serum antibody enzyme-linked immunosorbent assays were performed as previously described [114]. Briefly, microplates were coated with LCMV-infected baby hamster kidney (BHK) cell lysates overnight. Subsequently, nonspecific binding was blocked by coating microplates with 3% bovine serum albumin (BSA) in phosphate-buffered saline (PBS). Serial dilutions of serum were carried out in 1% BSA in PBS. After overnight incubation, plates were incubated with purified biotin-conjugated anti-mouse IgG, IgG1, or IgG2a (1030–08, 1070–08, 1080–08; Southern Biotech) antibodies for 2 hrs. Antibody detection was further performed using streptavidin–alkaline phosphatase (11089161001, Roche) for 1 hour and then alkaline phosphatase substrate solution containing 4-nitro-phenyl phosphate (N2765-50TAB, Sigma-Aldrich) for approximately 30min. A CLARIOstar Plus microplate reader was used to quantify the results.

Statistical analysis and graphing

All statistical analysis were performed using GraphPad Prism (La Jolla, CA) and used as appropriate for the data. The type of statistical test is listed in figure legends. Data was considered statistically significant is the p value$<$0.05. Graphs were made in GraphPad Prism (La Jolla, CA). Figure legends indicate if data shown is pooled from multiple studies or is from representative study.

DOI Dryad

10.5061/dryad.msbcc2g55) [115].

Supporting information

S1 Fig. Gene expression in CD8 T cell recluster. CD8 T cells were reclustered within Loupe software using aggregated file containing both PEP-WT and PEP-619WW data. tSNE visualizing Clusters 1–4 of CD8 T cell re-cluster analysis. Cluster 1 salmon, Cluster 2 light green, cluster 3 blue, and Cluster 4 light orange (A). Average gene expression of genes *Cd3e* (B), *Cd8b1* (C), *H2-Aa* (D), *H2-Ab1* (E), *H2-Eb1* (F), *Lyz2* (G), *Csfr1* (H) and *Cd19* (I). Gene expression shown in Log2 scale, range is on heat map scale for each tSNE plot.
(TIFF)

S2 Fig. PEP-619WW have more LCMV neutralizing antibodies 9 days post infection than PEP-WT. Serum from infected PEP-WT (black) and PEP-619WW (blue) taken at 0, 3, 9, 21, and 41 days post infection and measured for neutralizing IgG2A antibodies. Data shown from a 1: 1583 dilution. Representative experiment shown. SEM shown. *p$<$0.05; T-test at each

time point between genotypes.
(TIFF)

S3 Fig. Representative Gating Strategy for different immune cell populations presented in manuscript. Representative gating strategies to identify populations of interest presented throughout this manuscript. Populations are labeled on flow cytometry plots. Arrows indicated down gating of the population where they are drawn from. Gating strategies are also listed in figurelegends where the data appears.
(TIFF)

Acknowledgments

We thank Scripps Research and University of Kansas Flow Cytometry Core, Histology and Microscopy Core, and Vivarium staff for their expertise and assistance in this work. We also thank T. Fehr and C. Antunes (University of Kansas) for their careful reading and editing of this manuscript. Since the creation of the PEP-619WW mice, K. Mowen has passed away and is greatly missed.

Author Contributions

Conceptualization: Robin C. Orozco, John R. Teijaro, Linda A. Sherman.

Data curation: Robin C. Orozco, Kristi Marquardt, Isaraphorn Pratumchai, Anam Fatima Shaikh, Alain Domissy.

Formal analysis: Robin C. Orozco, Kristi Marquardt, Isaraphorn Pratumchai, Anam Fatima Shaikh, Alain Domissy.

Funding acquisition: Robin C. Orozco, Linda A. Sherman.

Methodology: Robin C. Orozco, Kristi Marquardt, Isaraphorn Pratumchai, Anam Fatima Shaikh, Alain Domissy.

Project administration: Robin C. Orozco, Linda A. Sherman.

Resources: Robin C. Orozco, Kerri Mowen, John R. Teijaro, Linda A. Sherman.

Supervision: Robin C. Orozco, John R. Teijaro, Linda A. Sherman.

Writing – original draft: Robin C. Orozco, Linda A. Sherman.

Writing – review & editing: Robin C. Orozco, Alain Domissy, John R. Teijaro, Linda A. Sherman.

References

1. Uffelmann E, Huang QQ, Munung NS, de Vries J, Okada Y, Martin AR, et al. Genome-wide association studies. Nature Reviews Methods Primers. 2021; 1(1):59. https://doi.org/10.1038/s43586-021-00056-9
2. Chiaroni-Clarke RC, Li YR, Munro JE, Chavez RA, Scurrah KJ, Pezic A, et al. The association of PTPN22 rs2476601 with juvenile idiopathic arthritis is specific to females. Genes Immun. 2015; 16 (7):495–8. Epub 20150820. https://doi.org/10.1038/gene.2015.32 PMID: 26291515.
3. Di Y, Zhong S, Wu L, Li Y, Sun N. The Association between PTPN22 Genetic Polymorphism and Juvenile Idiopathic Arthritis (JIA) Susceptibility: An Updated Meta-Analysis. Iran J Public Health. 2015; 44 (9):1169–75. PMID: 26587490.
4. Wang H, Wang Z, Rani PL, Fu X, Yu W, Bao F, et al. Identification of PTPN22, ST6GAL1 and JAZF1 as psoriasis risk genes demonstrates shared pathogenesis between psoriasis and diabetes. Exp Dermatol. 2017; 26(11):1112–7. Epub 20170825. https://doi.org/10.1111/exd.13393 PMID: 28603863.

5. Wang XH, Ma AG, Han XX, Chen L, Liang H, Aishan L, et al. Protein tyrosine phosphatase nonreceptor type 22 (PTPN22) gene single nucleotide polymorphisms and its interaction with T2DM on pulmonary tuberculosis in Chinese Uygur population. Oncotarget. 2017; 8(39):65601–8. Epub 20170715. https://doi.org/10.18632/oncotarget.19274 PMID: 29029456.

6. Gomez LM, Anaya JM, Gonzalez CI, Pineda-Tamayo R, Otero W, Arango A, et al. PTPN22 C1858T polymorphism in Colombian patients with autoimmune diseases. Genes Immun. 2005; 6(7):628–31. https://doi.org/10.1038/sj.gene.6364261 PMID: 16163373.

7. Burn GL, Svensson L, Sanchez-Blanco C, Saini M, Cope AP. Why is PTPN22 a good candidate susceptibility gene for autoimmune disease? FEBS Lett. 2011; 585(23):3689–98. Epub 20110420. https://doi.org/10.1016/j.febslet.2011.04.032 PMID: 21515266.

8. Armitage LH, Wallet MA, Mathews CE. Influence of PTPN22 Allotypes on Innate and Adaptive Immune Function in Health and Disease. Front Immunol. 2021; 12:636618. Epub 20210225. https://doi.org/10.3389/fimmu.2021.636618 PMID: 33717184.

9. Bottini N, Vang T, Cucca F, Mustelin T. Role of PTPN22 in type 1 diabetes and other autoimmune diseases. Semin Immunol. 2006; 18(4):207–13. Epub 20060511. https://doi.org/10.1016/j.smim.2006.03.008 PMID: 16697661.

10. Cohen S, Dadi H, Shaoul E, Sharfe N, Roifman CM. Cloning and characterization of a lymphoid-specific, inducible human protein tyrosine phosphatase, Lyp. Blood. 1999; 93(6):2013–24. PMID: 10068674.

11. Wang Y, Ewart D, Crabtree JN, Yamamoto A, Baechler EC, Fazeli P, et al. PTPN22 Variant R620W Is Associated With Reduced Toll-like Receptor 7-Induced Type I Interferon in Systemic Lupus Erythematosus. Arthritis Rheumatol. 2015; 67(9):2403–14. https://doi.org/10.1002/art.39211 PMID: 26018863.

12. Wallis AM, Wallace EC, Hostager BS, Yi Z, Houtman JCD, Bishop GA. TRAF3 enhances TCR signaling by regulating the inhibitors Csk and PTPN22. Sci Rep. 2017; 7(1):2081. Epub 20170518. https://doi.org/10.1038/s41598-017-02280-4 PMID: 28522807.

13. Bottini N, Peterson EJ. Tyrosine phosphatase PTPN22: multifunctional regulator of immune signaling, development, and disease. Annu Rev Immunol. 2014; 32:83–119. Epub 20131218. https://doi.org/10.1146/annurev-immunol-032713-120249 PMID: 24364806.

14. Vang T, Liu WH, Delacroix L, Wu S, Vasile S, Dahl R, et al. LYP inhibits T-cell activation when dissociated from CSK. Nat Chem Biol. 2012; 8(5):437–46. Epub 20120318. https://doi.org/10.1038/nchembio.916 PMID: 22426112.

15. Wang Y, Shaked I, Stanford SM, Zhou W, Curtsinger JM, Mikulski Z, et al. The autoimmunity-associated gene PTPN22 potentiates toll-like receptor-driven, type 1 interferon-dependent immunity. Immunity. 2013; 39(1):111–22. Epub 20130718. https://doi.org/10.1016/j.immuni.2013.06.013 PMID: 23871208.

16. Chang HH, Miaw SC, Tseng W, Sun YW, Liu CC, Tsao HW, et al. PTPN22 modulates macrophage polarization and susceptibility to dextran sulfate sodium-induced colitis. J Immunol. 2013; 191(5):2134–43. Epub 20130802. https://doi.org/10.4049/jimmunol.1203363 PMID: 23913970.

17. Sood S, Brownlie RJ, Garcia C, Cowan G, Salmond RJ, Sakaguchi S, et al. Loss of the Protein Tyrosine Phosphatase PTPN22 Reduces Mannan-Induced Autoimmune Arthritis in SKG Mice. J Immunol. 2016; 197(2):429–40. Epub 20160610. https://doi.org/10.4049/jimmunol.1502656 PMID: 27288531.

18. Salmond RJ, Brownlie RJ, Zamoyska R. Multifunctional roles of the autoimmune disease-associated tyrosine phosphatase PTPN22 in regulating T cell homeostasis. Cell Cycle. 2015; 14(5):705–11. https://doi.org/10.1080/15384101.2015.1007018 PMID: 25715232.

19. Dai X, James RG, Habib T, Singh S, Jackson S, Khim S, et al. A disease-associated PTPN22 variant promotes systemic autoimmunity in murine models. J Clin Invest. 2013; 123(5):2024–36. Epub 20130424. https://doi.org/10.1172/JCI66963 PMID: 23619366.

20. Hasegawa K, Martin F, Huang G, Tumas D, Diehl L, Chan AC. PEST domain-enriched tyrosine phosphatase (PEP) regulation of effector/memory T cells. Science. 2004; 303(5658):685–9. https://doi.org/10.1126/science.1092138 PMID: 14752163.

21. Ahmed R, Salmi A, Butler LD, Chiller JM, Oldstone MB. Selection of genetic variants of lymphocytic choriomeningitis virus in spleens of persistently infected mice. Role in suppression of cytotoxic T lymphocyte response and viral persistence. J Exp Med. 1984; 160(2):521–40. https://doi.org/10.1084/jem.160.2.521 PMID: 6332167.

22. Southern PJ, Blount P, Oldstone MB. Analysis of persistent virus infections by in situ hybridization to whole-mouse sections. Nature. 1984; 312(5994):555–8. https://doi.org/10.1038/312555a0 PMID: 6504163.

23. Wilsnack RE, Rowe WP. Immunofluorescent Studies of the Histopathogenesis of Lymphocytic Choriomeningitis Virus Infection. J Exp Med. 1964; 120(5):829–40. https://doi.org/10.1084/jem.120.5.829 PMID: 14247723.

24. Oldstone MBA, Ware BC, Horton LE, Welch MJ, Aiolfi R, Zarpellon A, et al. Lymphocytic choriomeningitis virus Clone 13 infection causes either persistence or acute death dependent on IFN-1, cytotoxic T lymphocytes (CTLs), and host genetics. Proc Natl Acad Sci U S A. 2018; 115(33):E7814–E23. Epub 20180730. https://doi.org/10.1073/pnas.1804674115 PMID: 30061383.

25. Sullivan BM, Teijaro JR, de la Torre JC, Oldstone MB. Early virus-host interactions dictate the course of a persistent infection. PLoS Pathog. 2015; 11(1):e1004588. Epub 20150108. https://doi.org/10.1371/journal.ppat.1004588 PMID: 25569216.

26. Teijaro JR, Ng C, Lee AM, Sullivan BM, Sheehan KC, Welch M, et al. Persistent LCMV infection is controlled by blockade of type I interferon signaling. Science. 2013; 340(6129):207–11. https://doi.org/10.1126/science.1235214 PMID: 23580529.

27. Zajac AJ, Blattman JN, Murali-Krishna K, Sourdive DJ, Suresh M, Altman JD, et al. Viral immune evasion due to persistence of activated T cells without effector function. J Exp Med. 1998; 188(12):2205–13. https://doi.org/10.1084/jem.188.12.2205 PMID: 9858507.

28. Maine CJ, Teijaro JR, Marquardt K, Sherman LA. PTPN22 contributes to exhaustion of T lymphocytes during chronic viral infection. Proc Natl Acad Sci U S A. 2016; 113(46):E7231–E9. Epub 20161031. https://doi.org/10.1073/pnas.1603738113 PMID: 27799548.

29. Jofra T, Di Fonte R, Hutchinson TE, Dastmalchi F, Galvani G, Battaglia M, et al. Protein tyrosine phosphatase PTPN22 has dual roles in promoting pathogen versus homeostatic-driven CD8 T-cell responses. Immunol Cell Biol. 2017; 95(2):121–8. Epub 20161011. https://doi.org/10.1038/icb.2016.92 PMID: 27725666.

30. Beura LK, Anderson KG, Schenkel JM, Locquiao JJ, Fraser KA, Vezys V, et al. Lymphocytic choriomeningitis virus persistence promotes effector-like memory differentiation and enhances mucosal T cell distribution. J Leukoc Biol. 2015; 97(2):217–25. Epub 20141113. https://doi.org/10.1189/jlb.1HI0314-154R PMID: 25395301.

31. Ciurea A, Klenerman P, Hunziker L, Horvath E, Odermatt B, Ochsenbein AF, et al. Persistence of lymphocytic choriomeningitis virus at very low levels in immune mice. Proc Natl Acad Sci U S A. 1999; 96(21):11964–9. https://doi.org/10.1073/pnas.96.21.11964 PMID: 10518559.

32. Sevilla N, Kunz S, McGavern D, Oldstone MB. Infection of dendritic cells by lymphocytic choriomeningitis virus. Curr Top Microbiol Immunol. 2003; 276:125–44. https://doi.org/10.1007/978-3-662-06508-2_6 PMID: 12797446.

33. Bergthaler A, Flatz L, Hegazy AN, Johnson S, Horvath E, Lohning M, et al. Viral replicative capacity is the primary determinant of lymphocytic choriomeningitis virus persistence and immunosuppression. Proc Natl Acad Sci U S A. 2010; 107(50):21641–6. Epub 20101122. https://doi.org/10.1073/pnas.1011998107 PMID: 21098292.

34. Ng CT, Sullivan BM, Oldstone MBA. The role of dendritic cells in viral persistence. Current Opinion in Virology. 2011; 1(3):160–6. https://doi.org/10.1016/j.coviro.2011.05.006 PMID: 21909344

35. Jamieson BD, Butler LD, Ahmed R. Effective clearance of a persistent viral infection requires cooperation between virus-specific Lyt2+ T cells and nonspecific bone marrow-derived cells. J Virol. 1987; 61(12):3930–7. https://doi.org/10.1128/JVI.61.12.3930-3937.1987 PMID: 3500329.

36. Matloubian M, Concepcion RJ, Ahmed R. CD4+ T cells are required to sustain CD8+ cytotoxic T-cell responses during chronic viral infection. J Virol. 1994; 68(12):8056–63. https://doi.org/10.1128/JVI.68.12.8056-8063.1994 PMID: 7966595.

37. Hu J, Wu J, Li Y, Wang Z, Tang J, Li Z, et al. Sclerostin domain-containing protein 1 is dispensable for the differentiation of follicular helper and follicular regulatory T cells during acute viral infection. Am J Transl Res. 2019; 11(6):3722–36. Epub 20190615. PMID: 31312383.

38. Kalekar LA, Mueller DL. Relationship between CD4 Regulatory T Cells and Anergy In Vivo. J Immunol. 2017; 198(7):2527–33. https://doi.org/10.4049/jimmunol.1602031 PMID: 28320913.

39. Andreatta M, Corria-Osorio J, Müller S, Cubas R, Coukos G, Carmona SJ. Interpretation of T cell states from single-cell transcriptomics data using reference atlases. Nature Communications. 2021; 12(1):2965. https://doi.org/10.1038/s41467-021-23324-4 PMID: 34017005

40. Elyahu Y, Hekselman I, Eizenberg-Magar I, Berner O, Strominger I, Schiller M, et al. Aging promotes reorganization of the CD4 T cell landscape toward extreme regulatory and effector phenotypes. Sci Adv. 2019; 5(8):eaaw8330. Epub 20190821. https://doi.org/10.1126/sciadv.aaw8330 PMID: 31457092.

41. Iyer SS, Latner DR, Zilliox MJ, McCausland M, Akondy RS, Penaloza-Macmaster P, et al. Identification of novel markers for mouse CD4(+) T follicular helper cells. Eur J Immunol. 2013; 43(12):3219–32. Epub 20131014. https://doi.org/10.1002/eji.201343469 PMID: 24030473.

42. Ciucci T, Vacchio MS, Gao Y, Tomassoni Ardori F, Candia J, Mehta M, et al. The Emergence and Functional Fitness of Memory CD4+ T Cells Require the Transcription Factor Thpok. Immunity. 2019; 50(1):91–105.e4. https://doi.org/10.1016/j.immuni.2018.12.019 PMID: 30638736

43. Lee J-K, Kannarkat GT, Chung J, Joon Lee H, Graham KL, Tansey MG. RGS10 deficiency ameliorates the severity of disease in experimental autoimmune encephalomyelitis. Journal of Neuroinflammation. 2016; 13(1):24. https://doi.org/10.1186/s12974-016-0491-0 PMID: 26831924

44. Ward-Kavanagh Lindsay K, Lin Wai W, Šedý John R, Ware Carl F. The TNF Receptor Superfamily in Co-stimulating and Co-inhibitory Responses. Immunity. 2016; 44(5):1005–19. https://doi.org/10.1016/j.immuni.2016.04.019 PMID: 27192566

45. Karlsson M, Zhang C, Méar L, Zhong W, Digre A, Katona B, et al. A single–cell type transcriptomics map of human tissues. Science Advances. 2021; 7(31):eabh2169. https://doi.org/10.1126/sciadv.abh2169 PMID: 34321199

46. Human Protein Atlas. proteinatlas.org.

47. Caserta S, Nausch N, Sawtell A, Drummond R, Barr T, Macdonald AS, et al. Chronic infection drives expression of the inhibitory receptor CD200R, and its ligand CD200, by mouse and human CD4 T cells. PLoS One. 2012; 7(4):e35466. Epub 20120409. https://doi.org/10.1371/journal.pone.0035466 PMID: 22496920.

48. Kretz-Rommel A, Qin F, Dakappagari N, Cofiell R, Faas SJ, Bowdish KS. Blockade of CD200 in the Presence or Absence of Antibody Effector Function: Implications for Anti-CD200 Therapy. The Journal of Immunology. 2008; 180(2):699–705. https://doi.org/10.4049/jimmunol.180.2.699 PMID: 18178807

49. Uehata T, Iwasaki H, Vandenbon A, Matsushita K, Hernandez-Cuellar E, Kuniyoshi K, et al. Malt1-Induced Cleavage of Regnase-1 in CD4+ Helper T Cells Regulates Immune Activation. Cell. 2013; 153(5):1036–49. https://doi.org/10.1016/j.cell.2013.04.034 PMID: 23706741

50. Komori HK, Hart T, LaMere SA, Chew PV, Salomon DR. Defining CD4 T cell memory by the epigenetic landscape of CpG DNA methylation. J Immunol. 2015; 194(4):1565–79. Epub 20150109. https://doi.org/10.4049/jimmunol.1401162 PMID: 25576597.

51. Hashimoto K, Kouno T, Ikawa T, Hayatsu N, Miyajima Y, Yabukami H, et al. Single-cell transcriptomics reveals expansion of cytotoxic CD4 T cells in supercentenarians. Proceedings of the National Academy of Sciences. 2019; 116(48):24242–51. https://doi.org/10.1073/pnas.1907883116 PMID: 31719197

52. Xue H-H, Kovanen PE, Pise-Masison CA, Berg M, Radovich MF, Brady JN, et al. IL-2 negatively regulates IL-7 receptor α chain expression in activated T lymphocytes. Proceedings of the National Academy of Sciences. 2002; 99(21):13759–64. https://doi.org/10.1073/pnas.212214999 PMID: 12354940

53. Schluns KS, Kieper WC, Jameson SC, Lefrançois L. Interleukin-7 mediates the homeostasis of naïve and memory CD8 T cells in vivo. Nat Immunol. 2000; 1(5):426–32. https://doi.org/10.1038/80868 PMID: 11062503.

54. Kakugawa K, Kojo S, Tanaka H, Seo W, Endo TA, Kitagawa Y, et al. Essential Roles of SATB1 in Specifying T Lymphocyte Subsets. Cell Reports. 2017; 19(6):1176–88. https://doi.org/10.1016/j.celrep.2017.04.038 PMID: 28494867

55. Notani D, Gottimukkala KP, Jayani RS, Limaye AS, Damle MV, Mehta S, et al. Global regulator SATB1 recruits beta-catenin and regulates T(H)2 differentiation in Wnt-dependent manner. PLoS Biol. 2010; 8(1):e1000296. Epub 20100126. https://doi.org/10.1371/journal.pbio.1000296 PMID: 20126258.

56. Readinger JA, Mueller KL, Venegas AM, Horai R, Schwartzberg PL. Tec kinases regulate T-lymphocyte development and function: new insights into the roles of Itk and Rlk/Txk. Immunol Rev. 2009; 228(1):93–114. https://doi.org/10.1111/j.1600-065X.2008.00757.x PMID: 19290923.

57. Mookerjee-Basu J, Kappes DJ. New ingredients for brewing CD4+T (cells): TCF-1 and LEF-1. Nature Immunology. 2014; 15(7):593–4. https://doi.org/10.1038/ni.2927 PMID: 24940944

58. Cano-Gamez E, Soskic B, Roumeliotis TI, So E, Smyth DJ, Baldrighi M, et al. Single-cell transcriptomics identifies an effectorness gradient shaping the response of CD4(+) T cells to cytokines. Nat Commun. 2020; 11(1):1801. Epub 20200414. https://doi.org/10.1038/s41467-020-15543-y PMID: 32286271.

59. Kuo H-H, Ahmad R, Lee GQ, Gao C, Chen H-R, Ouyang Z, et al. Anti-apoptotic Protein BIRC5 Maintains Survival of HIV-1-Infected CD4+ T Cells. Immunity. 2018; 48(6):1183–94.e5. https://doi.org/10.1016/j.immuni.2018.04.004 PMID: 29802019

60. Xu H, Yu J, Cui J, Chen Z, Zhang X, Zou Y, et al. Ablation of Survivin in T Cells Attenuates Acute Allograft Rejection after Murine Heterotopic Heart Transplantation by Inducing Apoptosis. Front Immunol. 2021; 12:710904. Epub 20210806. https://doi.org/10.3389/fimmu.2021.710904 PMID: 34421916.

61. Xing Z, Conway EM, Kang C, Winoto A. Essential role of survivin, an inhibitor of apoptosis protein, in T cell development, maturation, and homeostasis. J Exp Med. 2004; 199(1):69–80. Epub 20031229. https://doi.org/10.1084/jem.20031588 PMID: 14699085.

62. Kim C, Jin J, Ye Z, Jadhav RR, Gustafson CE, Hu B, et al. Histone deficiency and accelerated replication stress in T cell aging. J Clin Invest. 2021; 131(11). https://doi.org/10.1172/JCI143632 PMID: 34060486.

63. Strahler JR, Zhu XX, Hora N, Wang YK, Andrews PC, Roseman NA, et al. Maturation stage and proliferation-dependent expression of dUTPase in human T cells. Proc Natl Acad Sci U S A. 1993; 90 (11):4991–5. https://doi.org/10.1073/pnas.90.11.4991 PMID: 8389461.

64. Albrecht I, Niesner U, Janke M, Menning A, Loddenkemper C, Kuhl AA, et al. Persistence of effector memory Th1 cells is regulated by Hopx. Eur J Immunol. 2010; 40(11):2993–3006. Epub 20101027. https://doi.org/10.1002/eji.201040936 PMID: 21061432.

65. Denizot F, Brunet JF, Roustan P, Harper K, Suzan M, Luciani MF, et al. Novel structures CTLA-2 alpha and CTLA-2 beta expressed in mouse activated T cells and mast cells and homologous to cysteine proteinase proregions. Eur J Immunol. 1989; 19(4):631–5. https://doi.org/10.1002/eji.1830190409 PMID: 2786470.

66. Latta M, Mohan K, Issekutz TB. CXCR6 is expressed on T cells in both T helper type 1 (Th1) inflammation and allergen-induced Th2 lung inflammation but is only a weak mediator of chemotaxis. Immunology. 2007; 121(4):555–64. Epub 20070416. https://doi.org/10.1111/j.1365-2567.2007.02603.x PMID: 17437534.

67. Xu H, Williams MS, Spain LM. Patterns of expression, membrane localization, and effects of ectopic expression suggest a function for MS4a4B, a CD20 homolog in Th1 T cells. Blood. 2006; 107 (6):2400–8. Epub 20051117. https://doi.org/10.1182/blood-2005-08-3340 PMID: 16293604.

68. Crawford A, Angelosanto JM, Nadwodny KL, Blackburn SD, Wherry EJ. A role for the chemokine RANTES in regulating CD8 T cell responses during chronic viral infection. PLoS Pathog. 2011; 7(7): e1002098. Epub 20110721. https://doi.org/10.1371/journal.ppat.1002098 PMID: 21814510.

69. Yu Q, Chang H-C, Ahyi A-NN, Kaplan MH. Transcription Factor-Dependent Chromatin Remodeling of Il18r1 during Th1 and Th2 Differentiation1. The Journal of Immunology. 2008; 181(5):3346–52. https://doi.org/10.4049/jimmunol.181.5.3346 PMID: 18714006

70. Szabo SJ, Sullivan BM, Peng SL, Glimcher LH. Molecular mechanisms regulating Th1 immune responses. Annu Rev Immunol. 2003; 21:713–58. Epub 20011219. https://doi.org/10.1146/annurev.immunol.21.120601.140942 PMID: 12500979.

71. Tau G, Rothman P. Biologic functions of the IFN-gamma receptors. Allergy. 1999; 54(12):1233–51. https://doi.org/10.1034/j.1398-9995.1999.00099.x PMID: 10688427.

72. DeRogatis JM, Viramontes KM, Neubert EN, Tinoco R. PSGL-1 Immune Checkpoint Inhibition for CD4(+) T Cell Cancer Immunotherapy. Front Immunol. 2021; 12:636238. Epub 20210223. https://doi.org/10.3389/fimmu.2021.636238 PMID: 33708224.

73. Glatigny S, Duhen R, Oukka M, Bettelli E. Cutting edge: loss of α4 integrin expression differentially affects the homing of Th1 and Th17 cells. J Immunol. 2011; 187(12):6176–9. Epub 20111114. https://doi.org/10.4049/jimmunol.1102515 PMID: 22084440.

74. Wilson EB, Yamada DH, Elsaesser H, Herskovitz J, Deng J, Cheng G, et al. Blockade of chronic type I interferon signaling to control persistent LCMV infection. Science. 2013; 340(6129):202–7. https://doi.org/10.1126/science.1235208 PMID: 23580528.

75. Yao C, Sun H-W, Lacey NE, Ji Y, Moseman EA, Shih H-Y, et al. Single-cell RNA-seq reveals TOX as a key regulator of CD8+ T cell persistence in chronic infection. Nature Immunology. 2019; 20(7):890–901. https://doi.org/10.1038/s41590-019-0403-4 PMID: 31209400

76. Chen Y, Zander R, Khatun A, Schauder DM, Cui W. Transcriptional and Epigenetic Regulation of Effector and Memory CD8 T Cell Differentiation. Front Immunol. 2018; 9:2826. Epub 20181207. https://doi.org/10.3389/fimmu.2018.02826 PMID: 30581433.

77. Choi H, Song H, Jung YW. The Roles of CCR7 for the Homing of Memory CD8+ T Cells into Their Survival Niches. Immune Netw. 2020; 20(3):e20. Epub 20200520. https://doi.org/10.4110/in.2020.20.e20 PMID: 32655968.

78. Delpoux A, Marcel N, Hess Michelini R, Katayama CD, Allison KA, Glass CK, et al. FOXO1 constrains activation and regulates senescence in CD8 T cells. Cell Rep. 2021; 34(4):108674. https://doi.org/10.1016/j.celrep.2020.108674 PMID: 33503413.

79. Pritykin Y, van der Veeken J, Pine AR, Zhong Y, Sahin M, Mazutis L, et al. A unified atlas of CD8 T cell dysfunctional states in cancer and infection. Molecular Cell. 2021; 81(11):2477–93.e10. https://doi.org/10.1016/j.molcel.2021.03.045 PMID: 33891860

80. Jia X, Chua BY, Loh L, Koutsakos M, Kedzierski L, Olshansky M, et al. High expression of CD38 and MHC class II on CD8(+) T cells during severe influenza disease reflects bystander activation and trogocytosis. Clin Transl Immunology. 2021; 10(9):e1336. Epub 20210908. https://doi.org/10.1002/cti2.1336 PMID: 34522380.

81. Ruibal P, Oestereich L, Lüdtke A, Becker-Ziaja B, Wozniak DM, Kerber R, et al. Unique human immune signature of Ebola virus disease in Guinea. Nature. 2016; 533(7601):100–4. https://doi.org/10.1038/nature17949 PMID: 27147028.

82. Hua S, Lécuroux C, Sáez-Cirión A, Pancino G, Girault I, Versmisse P, et al. Potential role for HIV-specific CD38-/HLA-DR+ CD8+ T cells in viral suppression and cytotoxicity in HIV controllers. PLoS One. 2014; 9(7):e101920. Epub 20140707. https://doi.org/10.1371/journal.pone.0101920 PMID: 25000587.

83. Chandele A, Sewatanon J, Gunisetty S, Singla M, Onlamoon N, Akondy RS, et al. Characterization of Human CD8 T Cell Responses in Dengue Virus-Infected Patients from India. J Virol. 2016; 90 (24):11259–78. Epub 20161128. https://doi.org/10.1128/JVI.01424-16 PMID: 27707928.

84. Fox A, Le NM, Horby P, van Doorn HR, Nguyen VT, Nguyen HH, et al. Severe pandemic H1N1 2009 infection is associated with transient NK and T deficiency and aberrant CD8 responses. PLoS One. 2012; 7(2):e31535. Epub 20120220. https://doi.org/10.1371/journal.pone.0031535 PMID: 22363665.

85. Thevarajan I, Nguyen THO, Koutsakos M, Druce J, Caly L, van de Sandt CE, et al. Breadth of concomitant immune responses prior to patient recovery: a case report of non-severe COVID-19. Nat Med. 2020; 26(4):453–5. https://doi.org/10.1038/s41591-020-0819-2 PMID: 32284614.

86. Whitmire JK, Asano MS, Murali-Krishna K, Suresh M, Ahmed R. Long-term CD4 Th1 and Th2 memory following acute lymphocytic choriomeningitis virus infection. J Virol. 1998; 72(10):8281–8. https://doi.org/10.1128/JVI.72.10.8281-8288.1998 PMID: 9733872.

87. Greczmiel U, Krautler NJ, Pedrioli A, Bartsch I, Agnellini P, Bedenikovic G, et al. Sustained T follicular helper cell response is essential for control of chronic viral infection. Sci Immunol. 2017; 2(18). https://doi.org/10.1126/sciimmunol.aam8686 PMID: 29196449.

88. Wilson EB, Kidani Y, Elsaesser H, Barnard J, Raff L, Karp CL, et al. Emergence of distinct multiarmed immunoregulatory antigen-presenting cells during persistent viral infection. Cell Host Microbe. 2012; 11(5):481–91. https://doi.org/10.1016/j.chom.2012.03.009 PMID: 22607801.

89. Barber DL, Wherry EJ, Masopust D, Zhu B, Allison JP, Sharpe AH, et al. Restoring function in exhausted CD8 T cells during chronic viral infection. Nature. 2006; 439(7077):682–7. https://doi.org/10.1038/nature04444 PMID: 16382236

90. Sevilla N, McGavern DB, Teng C, Kunz S, Oldstone MB. Viral targeting of hematopoietic progenitors and inhibition of DC maturation as a dual strategy for immune subversion. J Clin Invest. 2004; 113 (5):737–45. https://doi.org/10.1172/JCI20243 PMID: 14991072.

91. Macal M, Lewis GM, Kunz S, Flavell R, Harker JA, Zuniga EI. Plasmacytoid dendritic cells are productively infected and activated through TLR-7 early after arenavirus infection. Cell Host Microbe. 2012; 11(6):617–30. https://doi.org/10.1016/j.chom.2012.04.017 PMID: 22704622.

92. Cagliani R, Sironi M. Pathogen-driven selection in the human genome. Int J Evol Biol. 2013; 2013:204240. Epub 20130304. https://doi.org/10.1155/2013/204240 PMID: 23533945.

93. Karlsson EK, Kwiatkowski DP, Sabeti PC. Natural selection and infectious disease in human populations. Nature Reviews Genetics. 2014; 15(6):379–93. https://doi.org/10.1038/nrg3734 PMID: 24776769

94. Vang T, Congia M, Macis MD, Musumeci L, Orrú V, Zavattari P, et al. Autoimmune-associated lymphoid tyrosine phosphatase is a gain-of-function variant. Nat Genet. 2005; 37(12):1317–9. Epub 20051106. https://doi.org/10.1038/ng1673 PMID: 16273109.

95. Fiorillo E, Orru V, Stanford SM, Liu Y, Salek M, Rapini N, et al. Autoimmune-associated PTPN22 R620W variation reduces phosphorylation of lymphoid phosphatase on an inhibitory tyrosine residue. J Biol Chem. 2010; 285(34):26506–18. Epub 20100609. https://doi.org/10.1074/jbc.M110.111104 PMID: 20538612.

96. Maine CJ, Marquardt K, Cheung J, Sherman LA. PTPN22 controls the germinal center by influencing the numbers and activity of T follicular helper cells. J Immunol. 2014; 192(4):1415–24. Epub 20140122. https://doi.org/10.4049/jimmunol.1302418 PMID: 24453256.

97. Orozco RC, Marquardt K, Mowen K, Sherman LA. Proautoimmune Allele of Tyrosine Phosphatase, PTPN22, Enhances Tumor Immunity. J Immunol. 2021; 207(6):1662–71. Epub 20210820. https://doi.org/10.4049/jimmunol.2100304 PMID: 34417261.

98. Fahey LM, Wilson EB, Elsaesser H, Fistonich CD, McGavern DB, Brooks DG. Viral persistence redirects CD4 T cell differentiation toward T follicular helper cells. J Exp Med. 2011; 208(5):987–99. Epub 20110502. https://doi.org/10.1084/jem.20101773 PMID: 21536743.

99. Metzler G, Dai X, Thouvenel CD, Khim S, Habib T, Buckner JH, et al. The Autoimmune Risk Variant PTPN22 C1858T Alters B Cell Tolerance at Discrete Checkpoints and Differentially Shapes the Naive Repertoire. J Immunol. 2017; 199(7):2249–60. Epub 20170811. https://doi.org/10.4049/jimmunol.1700601 PMID: 28801357.

100. Constant S, Pfeiffer C, Woodard A, Pasqualini T, Bottomly K. Extent of T cell receptor ligation can determine the functional differentiation of naive CD4+ T cells. Journal of Experimental Medicine. 1995; 182(5):1591–6. https://doi.org/10.1084/jem.182.5.1591 PMID: 7595230

101. Ise W, Totsuka M, Sogawa Y, Ametani A, Hachimura S, Sato T, et al. Naive CD4+ T Cells Exhibit Distinct Expression Patterns of Cytokines and Cell Surface Molecules on Their Primary Responses to Varying Doses of Antigen. The Journal of Immunology. 2002; 168(7):3242–50. https://doi.org/10.4049/jimmunol.168.7.3242 PMID: 11907078

102. Hornick EL, Wallis AM, Bishop GA. TRAF3 enhances type I interferon receptor signaling in T cells by modulating the phosphatase PTPN22. Sci Signal. 2022; 15(753):eabn5507. Epub 20220927. https://doi.org/10.1126/scisignal.abn5507 PMID: 36166512.

103. Lin X, Pelletier S, Gingras S, Rigaud S, Maine CJ, Marquardt K, et al. CRISPR-Cas9-Mediated Modification of the NOD Mouse Genome With Ptpn22R619W Mutation Increases Autoimmune Diabetes. Diabetes. 2016; 65(8):2134–8. Epub 20160426. https://doi.org/10.2337/db16-0061 PMID: 27207523.

104. Pratumchai I, Zak J, Huang Z, Min B, Oldstone MBA, Teijaro JR. B cell-derived IL-27 promotes control of persistent LCMV infection. Proc Natl Acad Sci U S A. 2022; 119(3). https://doi.org/10.1073/pnas.2116741119 PMID: 35022243.

105. Dobin A, Davis CA, Schlesinger F, Drenkow J, Zaleski C, Jha S, et al. STAR: ultrafast universal RNA-seq aligner. Bioinformatics. 2013; 29(1):15–21. Epub 20121025. https://doi.org/10.1093/bioinformatics/bts635 PMID: 23104886.

106. Levine JH, Simonds EF, Bendall SC, Davis KL, Amir el AD, Tadmor MD, et al. Data-Driven Phenotypic Dissection of AML Reveals Progenitor-like Cells that Correlate with Prognosis. Cell. 2015; 162(1):184–97. Epub 20150618. https://doi.org/10.1016/j.cell.2015.05.047 PMID: 26095251.

107. Bendall SC, Davis KL, Amir el AD, Tadmor MD, Simonds EF, Chen TJ, et al. Single-cell trajectory detection uncovers progression and regulatory coordination in human B cell development. Cell. 2014; 157(3):714–25. https://doi.org/10.1016/j.cell.2014.04.005 PMID: 24766814.

108. Blondel VD, Guillaume J-L, Lambiotte R, Lefebvre E. Fast unfolding of communities in large networks. Journal of Statistical Mechanics: Theory and Experiment. 2008; 2008(10):P10008. https://doi.org/10.1088/1742-5468/2008/10/P10008

109. Stassen SV, Siu DMD, Lee KCM, Ho JWK, So HKH, Tsia KK. PARC: ultrafast and accurate clustering of phenotypic data of millions of single cells. Bioinformatics. 2020; 36(9):2778–86. https://doi.org/10.1093/bioinformatics/btaa042 PMID: 31971583.

110. Malkov YA, Yashunin DA. Efficient and Robust Approximate Nearest Neighbor Search Using Hierarchical Navigable Small World Graphs. IEEE Trans Pattern Anal Mach Intell. 2020; 42(4):824–36. Epub 20181228. https://doi.org/10.1109/TPAMI.2018.2889473 PMID: 30602420.

111. Traag VA, Waltman L, van Eck NJ. From Louvain to Leiden: guaranteeing well-connected communities. Sci Rep. 2019; 9(1):5233. Epub 20190326. https://doi.org/10.1038/s41598-019-41695-z PMID: 30914743.

112. Colin Megill BM, Charlotte Weaver, Sidney Bell, Severiano Badajoz, Matt Weiden, Justin Kiggins, Jeremy Freeman, fionagriffin, bmccandless, Marcus Kinsella, Snyk bot, Prete, Philipp A., Marcio von Muhlen, James Taylor, Isaac Virshup, Gökçen Eraslan, GenevieveHaliburton, & Alex Wolf. chanzuckerberg/cellxgene: Release 0.15.0 (0.15.0). Zenodo. 2020. https://doi.org/10.5281/zenodo.3710410.

113. Nguyen T-M, Shafi A, Nguyen T, Draghici S. Identifying significantly impacted pathways: a comprehensive review and assessment. Genome Biology. 2019; 20(1):203. https://doi.org/10.1186/s13059-019-1790-4 PMID: 31597578

114. Huang Z, Kang SG, Li Y, Zak J, Shaabani N, Deng K, et al. IFNAR1 signaling in NK cells promotes persistent virus infection. Sci Adv. 2021; 7(13). Epub 20210326. https://doi.org/10.1126/sciadv.abb8087 PMID: 33771858.

115. Orozco RC, Marquardt K., Pratumchai I., Shaikh A.F., Mowen K., Domissy A., Teijaro J.R., Sherman L.A. Autoimmunity-associated allele of tyrosine phosphatase gene PTPN22 enhances anti-viral immunity In: Dryad, editor. 2023.